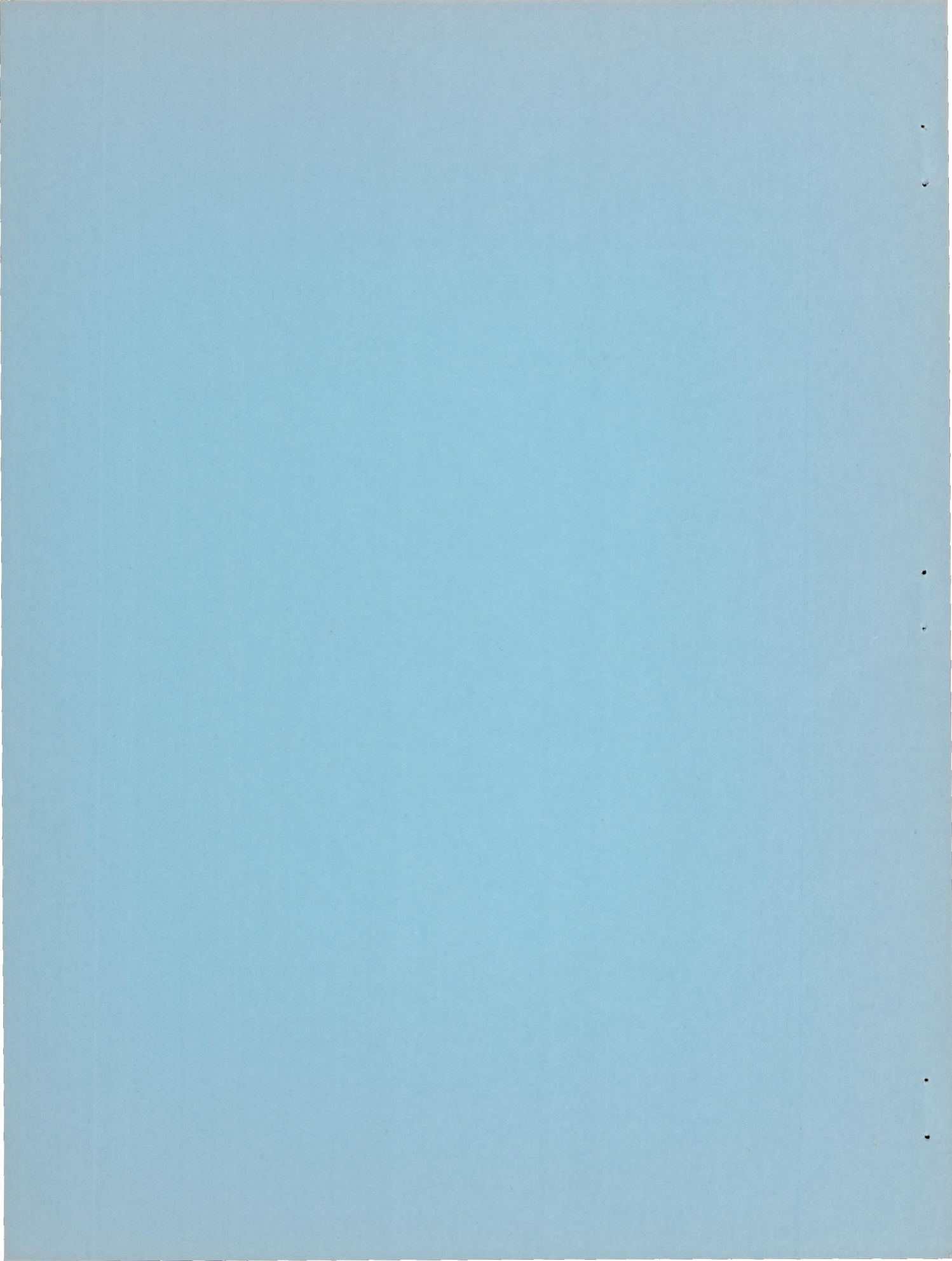NACA RM L54I13

NACA

RESEARCH MEMORANDUM

COMPARISON OF LOW-SPEED ROTOR AND CASCADE PERFORMANCE FOR

MEDIUM-CAMBER NACA 65-$(C_{l_0}A_{10})$10 COMPRESSOR-BLADE

SECTIONS OVER A WIDE RANGE OF ROTOR

BLADE-SETTING ANGLES AT SOLIDITIES

OF 1.0 AND 0.5

By George C. Ashby, Jr.

Langley Aeronautical Laboratory
Langley Field, Va.

NATIONAL ADVISORY COMMITTEE
FOR AERONAUTICS
WASHINGTON

December 27, 1954
Declassified September 24, 1956

NATIONAL ADVISORY COMMITTEE FOR AERONAUTICS

RESEARCH MEMORANDUM

COMPARISON OF LOW-SPEED ROTOR AND CASCADE PERFORMANCE FOR

MEDIUM-CAMBER NACA $65\text{-}\left(C_{l_0}A_{10}\right)10$ COMPRESSOR-BLADE

SECTIONS OVER A WIDE RANGE OF ROTOR

BLADE-SETTING ANGLES AT SOLIDITIES

OF 1.0 AND 0.5

By George C. Ashby, Jr.

SUMMARY

A medium-camber compressor rotor having NACA $65\text{-}\left(C_{l_0}A_{10}\right)10$ blades
was tested in a low-speed 28-inch test blower. The tests were made at
solidities of 1.0 and 0.5 without guide vanes or stators over a wide
range of blade-setting angles and quantity flow rates. The measured
overall and blade-element performance was compared with the performance
estimated from cascade data to extend the correlation of cascade and
compressor-rotor data over a broad range of blade-setting angles.

As a result of this investigation, the rotor turning angles were
generally found to be 1° to $2\frac{1}{2}^{\circ}$ higher than the cascade in the region of
the annulus free of wall boundary-layer effects. Estimates of efficiency
at the design angle of attack using lift-drag ratios from cascade data
were found to agree very well with measured values except in the hub and
tip regions influenced by wall boundary-layer effects. The rotor oper-
ated with an efficiency greater than 85 percent at both solidities over
a wide range of angles of attack for all blade-setting angles.

INTRODUCTION

Two-dimensional cascade data obtained in a porous-wall test facility
are extensively used in the design of axial-flow compressors. Since the
flow in axial-flow compressors is three-dimensional, a correlation between
cascade and compressor-rotor data is required. Pressure distributions

and turning angles measured for a rotor have been shown in reference 1 to be similar to those measured in cascade at the design angle of attack. Reference 2 indicates that rotor performance data can be estimated accurately from cascade data for a wide variety of conditions. The purpose of the present investigation is to further the establishment of a correlation between low-speed cascade and compressor-rotor data over a wide range of blade-setting angles.

A rotor having medium-camber NACA 65-series airfoil sections, was tested without guide vanes or stators over a wide range of blade-setting angles in a low-speed 28-inch test blower. Measured overall and blade-element performance values were compared with values estimated by using two-dimensional porous-wall cascade data. To facilitate this work, the rotor was designed with constant solidity along the radius.

SYMBOLS

C_{l_o} isolated airfoil design lift coefficient

D diameter, ft

M mass flow, slugs/sec

n rotor speed, rps

p static pressure, lb/ft^2

P total pressure, lb/ft^2

Q quantity flow of air, ft^3/sec

U rotor-blade velocity, ft/sec

V airspeed respective to stationary casing, ft/sec

α angle of attack relative to blade chord, deg

β air angle relative to blade, measured from axis, deg

ξ blade-setting angle, angle between blade chord and rotor axis, deg

η adiabatic efficiency, percent

θ air turning angle, deg

ρ air density, slugs/ft^3

σ solidity, blade chord divided by blade gap

Φ quantity flow coefficient, $Q/nD_t{}^3$

Ψ_S static-pressure-rise coefficient, $\dfrac{p_2 - p_1}{\frac{1}{2}\rho U_t{}^2}$

Ψ_T total-pressure-rise coefficient, $\dfrac{P_2 - P_1}{\frac{1}{2}\rho U_t{}^2}$

Subscripts:

1   upstream of blade row

2   downstream of blade row

a   axial direction

d   design condition

m   mean-radius section

t   tip section

ROTOR DESIGN AND TEST PROGRAM

The rotor blades were designed so that the exit tangential velocity was inversely proportional to the radius (free-vortex condition) and had medium-camber NACA 65-$(C_{l_0}A_{10})$10 airfoil sections. The blade chord was varied along the blade span to provide constant solidity. The following table presents the design details:

Station	NACA section	α_d, deg	θ_d, deg	β_{1_d}, deg	β_{2_d}, deg	ξ_d, deg	σ_d	Radius, in.
Hub	65$(17A_{10})$10	16.0	26.0	48.9	22.9	32.9	1.00	10.91
Mean	65$(12A_{10})$10	12.5	18.8	52.5	33.7	40.0	1.00	12.41
Tip	65$(8.5A_{10})$10	10.0	13.8	55.6	41.8	45.6	1.00	13.91

A photograph of the rotor is presented as figure 1. The rotor was tested at low speed in the 28-inch test blower described in reference 2. Downstream radial surveys of flow direction and static and total pressure were made with prism probes of the type described in reference 3. Prior to these downstream surveys, radial upstream surveys were made with a similar probe to check the inlet flow distribution. These upstream surveys were used in conjunction with the downstream surveys in the final calculations of rotor performance. The solidity was changed by varying the number of blades. For solidities of 1.0 and 0.5, 26 and 13 blades were used, respectively. The tests were made over a range of flow coefficients from wide open throttle to surge at each of several blade-setting angles at solidities of 1.0 and 0.5. The blade-setting angles based on mean radius conditions were $\xi_d + 17.5^o$, $\xi_d + 7.5^o$, ξ_d, $\xi_d - 7.5^o$, and $\xi_d - 15^o$ for $\sigma = 1.0$. The same settings, excluding the $\xi_d - 15^o$ condition, were tested at $\sigma = 0.5$. The value of ξ_d for $\sigma = 0.5$ was 44.3^o compared with 40.0^o for $\sigma = 1.0$. The blade attachment was such that from 19 percent of chord to 76 percent there was no hub clearance because the hub shank, which was 1.5 inches in diameter, was integral with the blade. At the highest blade-setting angle the hub clearance at the leading edge was 0.048 inch and decreased to 0.020 inch near the leading-edge side of the shank; whereas the trailing-edge clearance was 0.030 inch and decreased to 0.015 inch near the trailing-edge side of the shank. These clearances decrease with decreasing setting angle and were very small at design setting angles and below. Test Reynolds numbers, based on mean-radius chord, ranged from approximately 300,000 to 550,000. The rotor speed was 2,000 rpm for all configurations except the $\xi_d - 15^o$, $\sigma = 1.0$ condition. Because of power limitations, this configuration was tested at 1,600 rpm.

The measured flow angles are considered to be accurate to $\pm 1/2^o$. The testing speed was held within ± 5 rpm by using a tachometer and stroboscope. The variation between mass flow obtained from upstream and downstream measurements for all the tests presented herein is indicated in figure 2. The maximum difference between mass-flow measurements made upstream and downstream of the rotor is almost always less than 4 percent, and the average difference is approximately 1 percent. All flow coefficients were obtained from the upstream measurements which are believed to be correct. On the basis of these testing accuracies, it is believed that efficiencies and pressure-rise coefficients are accurate to within ± 2 to ± 3 percent.

RESULTS AND DISCUSSION

Overall Rotor Performance

Efficiency and pressure-rise coefficients.- Measured adiabatic efficiency and pressure-rise coefficients were obtained by mass weighting the results obtained from the surveys. They are plotted against flow coefficient for all blade-setting angles at both solidities in figures 3 and 4. Pressure-rise coefficients at the design blade-setting angle, estimated by using cascade data, are also presented. The flagged test points indicate that the rotor was operating with an audible rumble which is considered to result from partial-span rotating stall, that is, a stall region covering part of the span which rotates in the same direction as the rotor at a speed anywhere from 25 to 85 percent of the rotor speed. Partial-span rotating stall usually results in a continuous drop in efficiency and pressure-rise coefficient with decreasing flow coefficient as indicated for the $\xi_d - 15^o$ blade setting at $\sigma = 1.0$ and the $\xi_d - 7.5^o$ blade setting at $\sigma = 0.5$. (See refs. 4 and 5.)

High efficiency was obtained over a wide range of quantity flow coefficients at each blade-setting angle. Maximum efficiencies of approximately 0.95 were obtained for all blade-setting-angle and solidity conditions. For $\sigma = 1.0$, the efficiency is 0.85 or greater for flow-coefficient ranges of 0.17, 0.32, 0.46, 0.54, and 0.55 as the blade-setting angle decreased from $\xi_d + 17.5^o$ to $\xi_d - 15^o$. These flow-coefficient ranges correspond to ranges of angle of attack of approximately 10°, 16°, 19°, 20°, and 16°, respectively. At $\sigma = 0.5$, the ranges of flow coefficient for efficiencies of 0.85 or greater were 0.23, 0.31, 0.35, and 0.32 as the blade-setting angle decreased from $\xi_d + 17.5^o$ to $\xi_d - 7.5^o$ with corresponding angle-of-attack ranges of 13°, 15°, 16°, and 12°. Hence, for the same design inlet-angle conditions, the lower solidity exhibited a smaller angle-of-attack operating range for all inlet angles except the highest, which corresponds to $\xi_d + 17.5^o$ setting angles. At this condition, the design loading at $\sigma = 1.0$ was so high that rotor stall occurred very close to the design angle of attack and, as a result, the angle-of-attack range at $\sigma = 1.0$ was less than that associated with $\sigma = 0.5$.

The estimated pressure-rise coefficients at the design blade-setting angle were calculated by assuming no losses; therefore, they would normally be higher than measured values. However, the turning angles obtained in the rotor tests were higher than the cascade-estimated values (to be discussed later) and evidently compensate for the exclusion of losses since good agreement was obtained. This agreement substantiates the same result reported in reference 2.

Comparison of overall efficiency range with that of rotor of
reference 2.- Since the rotor reported in reference 2 was similar to the
subject rotor, it was decided to compare the range of high efficiencies
of the two. The following table presents the major design parameters of
the two rotors:

Rotor	β_{1_d}, deg			θ_d, deg			C_{l_o}			σ		
	Hub	Mean	Tip	Hub	Mean	Tip	Hub	Mean	Tip	Hub	Mean	Tip
Present investigation	48.9	52.5	55.6	26.0	18.8	13.8	1.7	1.2	0.85	1.0	1.0	1.0
Reference 2	48.8	52.4	55.5	24.1	17.4	12.9	1.35	1.13	.85	1.14	1.00	.89

The design loading differences are small. The solidity variation and the
variation in hub camber are the most significant differences.

Since the ranges of high efficiency and not absolute values of
efficiency are of primary concern (the differences in the levels of
efficiency between the two rotors were within measuring accuracy except
for the $\xi_d + 7.5^o$, $\sigma = 1.0$ condition where the level for the rotor of
ref. 2 was $4\frac{1}{2}$ percent higher), η/η_{peak} was plotted for ease of com-
parison. Figure 5 shows this comparison at both solidities for the
setting-angle range of reference 2. At $\sigma = 1.0$, the differences in the
ranges of high efficiency are negligible. At $\sigma = 0.5$, the rotor of the
present investigation showed a somewhat improved range on the high-flow
side for each of the blade settings examined. This improvement is prob-
ably due to the higher tip solidity which existed in the rotor of the
present investigation (0.50 compared with 0.45).

Comparison Between Measured and Estimated Section

Efficiencies Near Design Angle of Attack

Section efficiencies were estimated by the procedure presented in
reference 6 by using cascade section lift-drag ratios obtained from
reference 7. The equation when applied to this type of investigation is
given in reference 2. Figures 6 and 7 compare estimated and measured
values across the annulus near the design angle of attack for $\xi_d + 7.5^o$
and ξ_d at $\sigma = 1.0$ and ξ_d at $\sigma = 0.5$, respectively. For the design
conditions examined, the estimated and measured efficiencies agree very

well except for the regions affected by secondary flows, wall boundary layers, and tip clearance. Hence, these comparisons at the design angle of attack indicate that cascade lift-drag ratios can be used to estimate rotor section efficiencies in the region not influenced by end effects with reasonable accuracy.

Figures 8 and 9 are presented to compare the estimated overall rotor efficiency with the measured values. It was found that the estimated overall efficiency was generally higher than that measured. This result is to be expected since, as mentioned previously, the estimated efficiency did not include the end-wall boundary-layer effects. At the lower blade loading conditions, (that is, high flow rates) the end-wall boundary-layer effects would be reduced and closer agreement between the two efficiencies would be expected. This is evident in figures 8 and 9.

Comparison Between Low-Speed Rotor and Cascade Turning Angles

Figures 10 and 11 present detailed comparisons of cascade and rotor turning angles at three radial stations for two solidities (1.0 and 0.5). The three stations chosen were an inboard section (radius, 11.26 in.), the mean section (radius, 12.41 in.), and an outboard section (radius, 13.56 in.). The inboard and outboard stations were almost 12 percent of the span from the inner and outer casings, respectively. The sections were selected to be outside the wall boundary layers; however, the inboard section was found later to be in the hub boundary-layer region. In figures 10 and 11, the angle-of-attack scale for each curve has been shifted along the abscissa a number of scale units proportional to the change in blade-setting angle. The slopes of the curves obtained from cascade and rotor tests are very similar. For the mean and outboard sections, the rotor turning angles were generally 1° to $2\frac{1}{2}^\circ$ higher than cascade values at both solidities. The direction of this result is consistent with the results for the rotor reported in reference 2 where the rotor turning angles were found to be 1° to $1\frac{1}{2}^\circ$ higher than cascade values. At the inboard section, the rotor turning angles were very close to the cascade turning angles except at $\sigma = 1.0$ where at the lower blade-setting angles they were about 2° to 3° low. This reduction in turning angle in the rotor with decreasing setting angle is not attributable to any hub clearance effect since the hub clearance is very small at the lower setting angles.

To determine whether the reduction resulted because of the hub boundary-layer effects, the spanwise variations of rotor measured turning angles and those estimated from cascade for $\xi_d + 7.5$, ξ_d, and $\xi_d - 7.5^\circ$ at $\sigma = 1.0$ and 0.5 are presented in figures 12 and 13. For the $\sigma = 1.0$ condition (fig. 12) the inboard station appeared to be in or close to the hub boundary-layer region. For the $\xi_d - 7.5^\circ$ blade-setting angle where

the rotor turning at the inboard station was considerably less than the cascade data, the inboard station was rather deeply imbedded in the hub boundary-layer region. For $\sigma = 0.5$, a similar but less severe trend of the hub boundary layer influencing the inboard turning angles is shown in figure 13. Cascade data were not extensive enough to provide estimated values for the outboard section at $\alpha_m = 7.25^{\circ}$, $\xi_d + 7.5^{\circ}$ and the inboard section at $\alpha_m = 8.25^{\circ}$, $\xi_d - 7.5^{\circ}$ (fig. 13). Hence, it appears that for all sections outside of the wall boundary-layer regions the rotor turning angles were generally from 1° to $2\frac{1}{2}^{\circ}$ higher than those obtained in cascade at the same conditions.

Figure 14 presents rotor test data as cross plots of turning-angle data against air inlet angle and angle of attack in carpet-plot form for the radial stations corresponding to cambers of 1.0, 1.2, and 1.4. For each value of C_{l_o} the angle-of-attack scales are shifted along the abscissa a number of scale units proportional to the changes in inlet angle. Given combinations of α and β are shifted along the abscissa a number of scale units proportional to the changes in C_{l_o}. Lines of constant α and β have been drawn. Interpolations for intermediate angles of attack, air inlet angles, and cambers are to be done along the abscissa. (Further discussion of carpet plotting is contained in ref. 8.) The radial stations corresponding to the three cambers were all outside of the wall boundary-layer regions except for the radial station corresponding to $C_{l_o} = 1.4$ at $\sigma = 1.0$. This station at $\sigma = 1.0$ was sometimes in the outer portion of the hub boundary-layer region as may be seen in figure 12 at the lowest blade-setting angle, $\xi_d - 7.5^{\circ}$. These figures are provided to facilitate the use of the rotor data for design purposes.

Detailed Blade Section Performance

To provide detailed section data for further analysis, the significant section performance parameters, that is, section efficiency, static and total pressure-rise coefficients, axial-velocity ratios, and flow coefficients, are presented at the inboard, mean, and outboard stations for all the blade-setting angles at both solidities. (See figs. 15 to 18.) As may be seen in figures 15 and 16, the inboard station generally had considerably lower efficiencies than the mean or outboard stations near design angle of attack. The axial-velocity ratios corresponding to these lower efficiencies (figs. 17(a) and 18(a)) were generally low, indicating an increase in hub boundary-layer thickness across the blade row. These effects were most pronounced for the higher blade-setting angles where the hub clearance has increased. These observations further substantiate the comment discussed previously in the section on turning angles, namely, that the inboard station was in the hub boundary-layer region. The

blockage of the flow at the hub by the increased thickness of the boundary layer across the blade row results in a shift of the flow toward the tip. This shift of flow toward the tip manifests itself in higher axial-velocity ratios at the mean section.

Some reduction in efficiency between the mean and outboard section existed at the higher blade-setting-angle conditions.

CONCLUSIONS

An investigation of a medium-camber NACA 65-series compressor rotor has been conducted over a range of blade-setting angles, flow rates, and solidities. The measured overall and blade-element performance has been compared with values estimated from cascade data. As a result of this investigation, the following conclusions are made:

1. The flow turning angles produced by the rotor were generally found to be 1° to $2\frac{1}{2}^\circ$ higher than cascade values for all blade sections unaffected by wall boundary layers.

2. For the design conditions compared, the section efficiencies estimated by using cascade lift-drag ratios were in reasonably good agreement with measured values except in the hub and tip regions influenced by wall boundary-layer effects.

3. The rotor operated with high efficiency over a wide range of angle of attack for each of the blade-setting angles at both solidities.

Langley Aeronautical Laboratory,
    National Advisory Committee for Aeronautics,
        Langley Field, Va., September 3, 1954.

REFERENCES

1. Westphal, Willard R., and Godwin, William R.: Comparison of NACA
   65-Series Compressor-Blade Pressure Distributions and Performance
   in a Rotor and in Cascade. NACA RM L51H20, 1951.

2. Schulze, Wallace M., Erwin, John R., and Ashby, George C., Jr.: NACA
   65-Series Compressor Rotor Performance With Varying Annulus-Area
   Ratio, Solidity, Blade Angle, and Reynolds Number and Comparison
   With Cascade Results. NACA RM L52L17, 1953.

3. Schulze, Wallace M., Ashby, George C., Jr., and Erwin, John R.:
   Several Combination Probes for Surveying Static and Total Pressure
   and Flow Direction. NACA TN 2830, 1952.

4. Huppert, Merle C., and Benser, William A.: Some Stall and Surge
   Phenomena in Axial-Flow Compressors. Jour. Aero. Sci., vol. 20,
   no. 12, Dec. 1953, pp. 835-845.

5. Iura, T., and Rannie, W. D.: Observations of Propagating Stall in
   Axial-Flow Compressors. Rep. No. 4. (Contract N6 - ORI - 102 Task
   Order IV), Mech. Eng. Lab., C.I.T., Apr. 1953.

6. Sinnette, John T., Jr.: Analysis of the Effect of Basic Design
   Variables on Subsonic Axial-Flow-Compressor Performance. NACA
   Rep. 901, 1948.

7. Herrig, L. Joseph, Emery, James C., and Erwin, John R.: Systematic
   Two-Dimensional Cascade Tests of NACA 65-Series Compressor Blades
   at Low Speeds. NACA RM L51G31, 1951.

8. Felix, A. Richard: Summary of 65-Series Compressor-Blade Low-Speed
   Cascade Data by Use of the Carpet-Plotting Technique. NACA
   RM L54H18a, 1954.
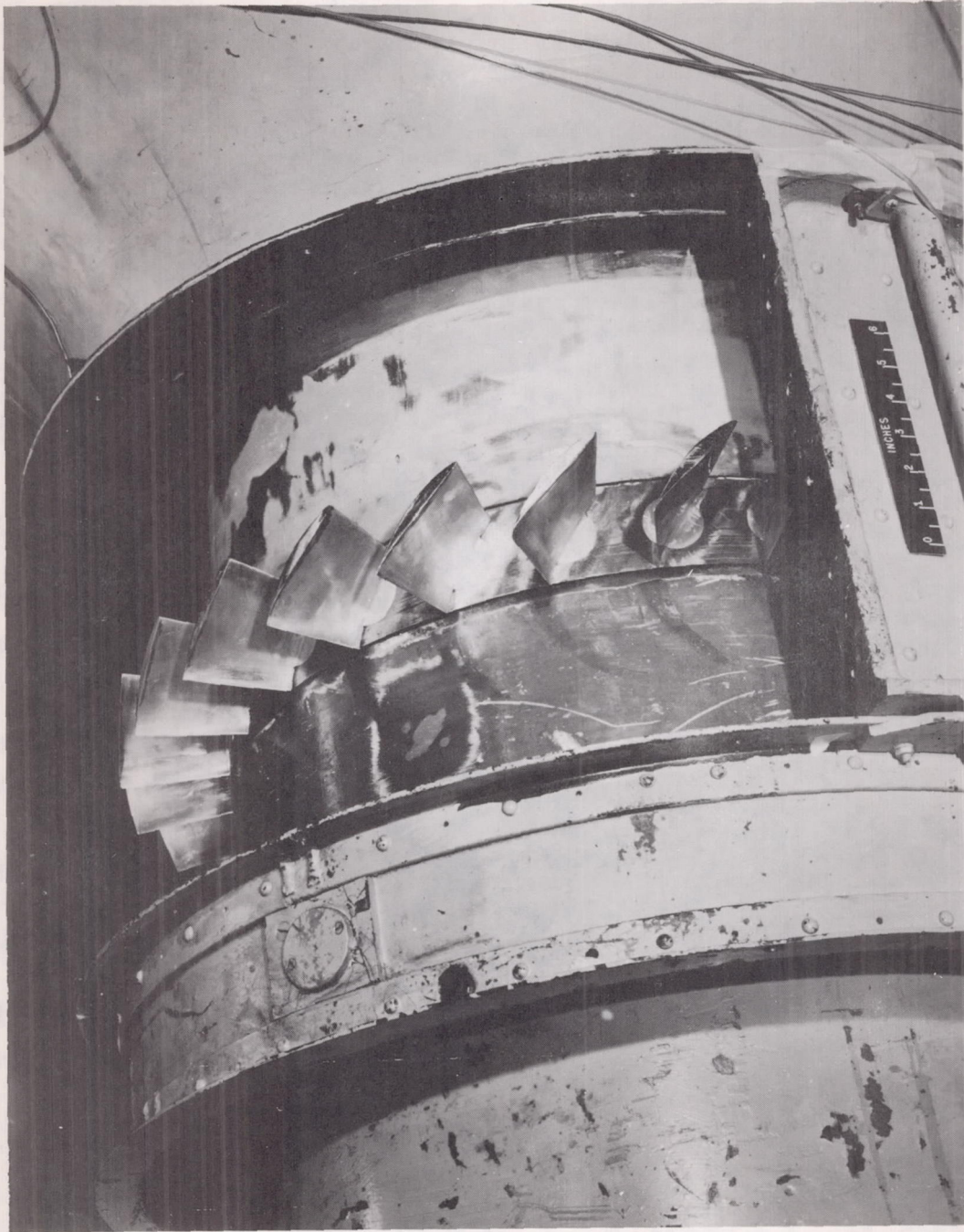
L-85899

Figure 1.- Rotor used in investigation.
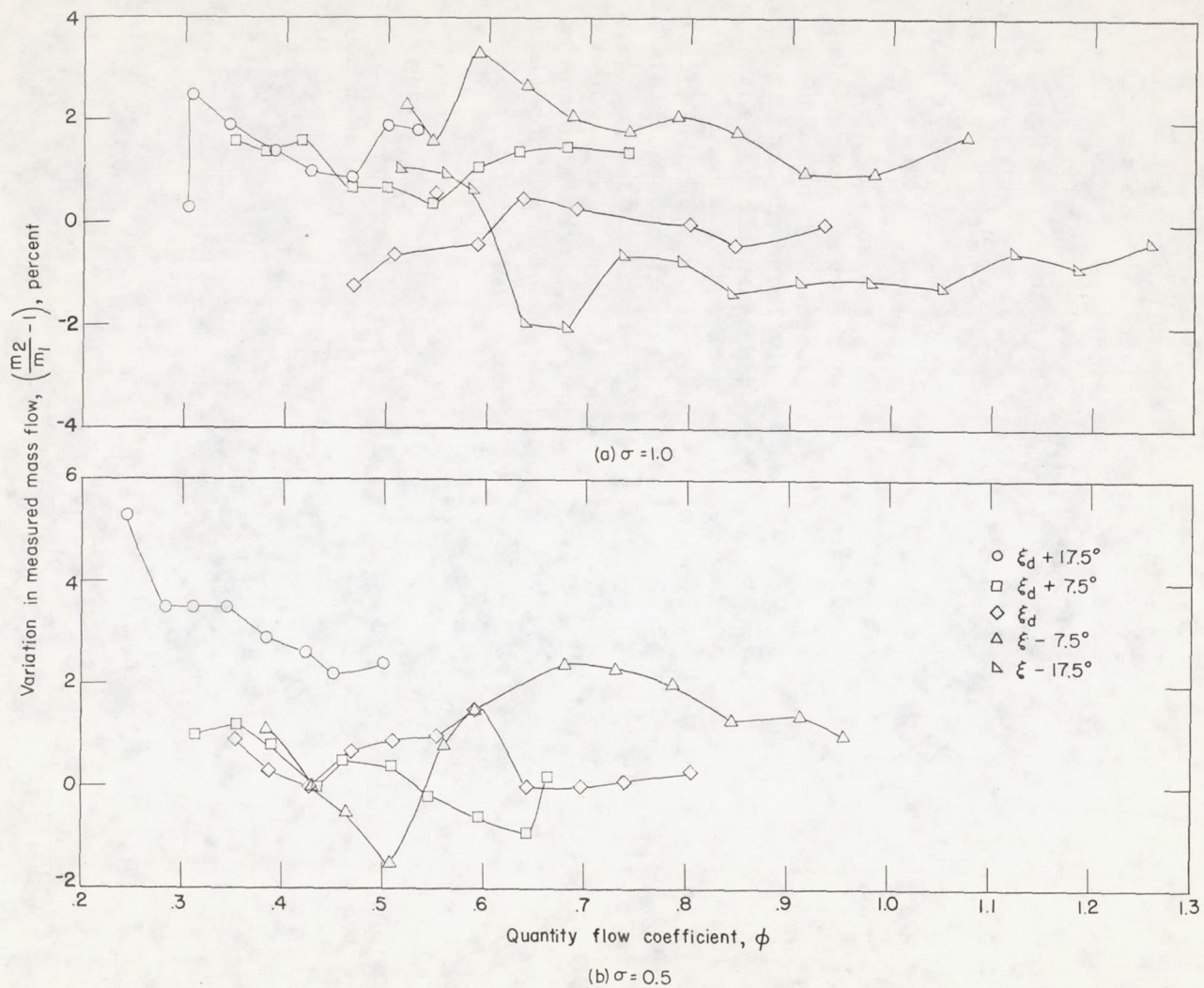
Figure 2.- Variation in mass flow as measured upstream and downstream
of rotor.
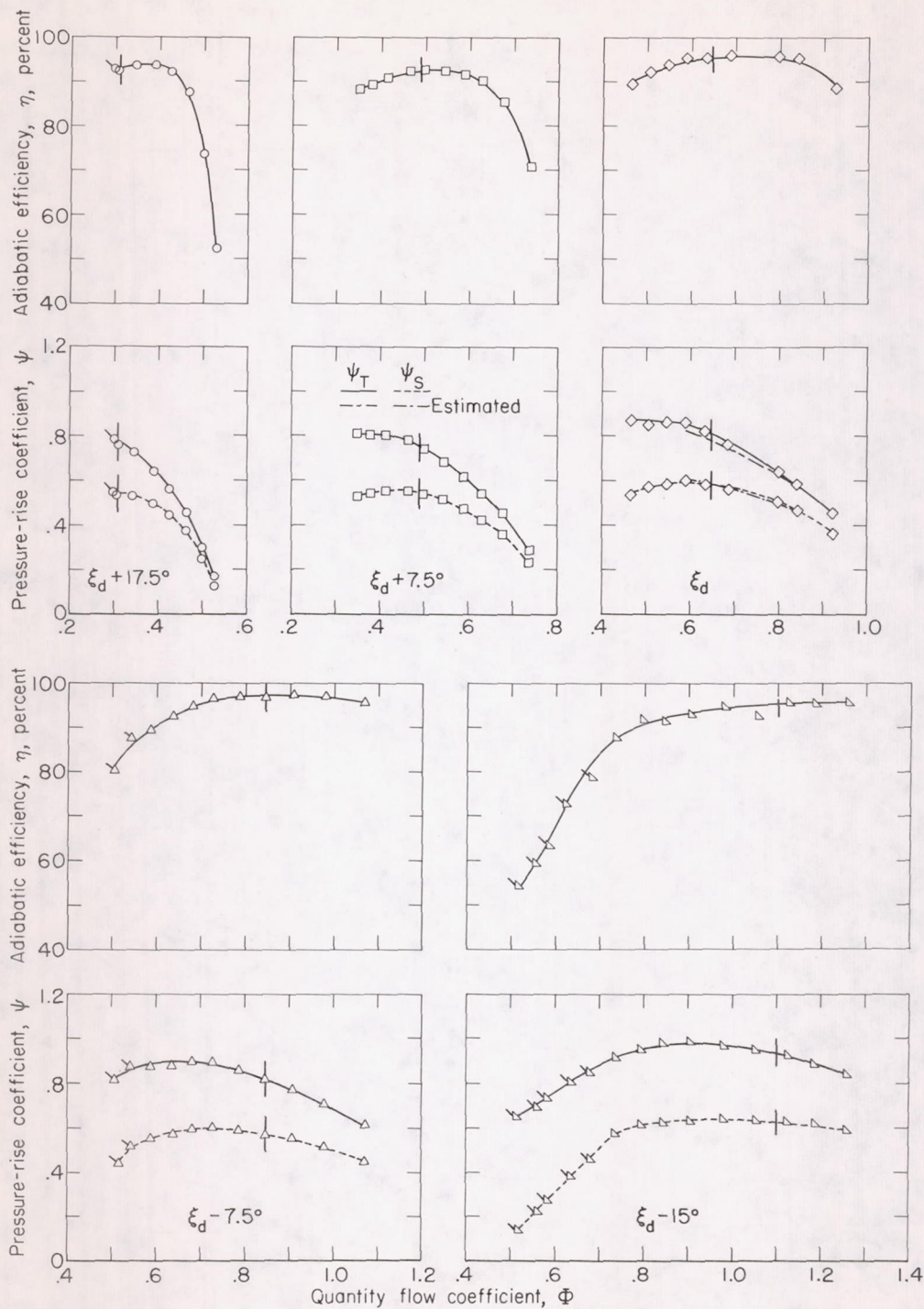
Figure 3.- Variation of adiabatic efficiency and total- and static-
pressure-rise coefficients with quantity flow coefficient at several
blade-setting angles and σ = 1.0. Vertical lines across curves
indicate design angle of attack. Flagged symbols indicate audible
partial-span rotating stall.

Figure 4.- Variation of adiabatic efficiency and total- and static-pressure-rise coefficients with quantity flow coefficient at several blade-setting angles and $\sigma = 0.5$. Vertical lines across curves indicate design. Flagged symbols indicate audible partial-span rotating stall.
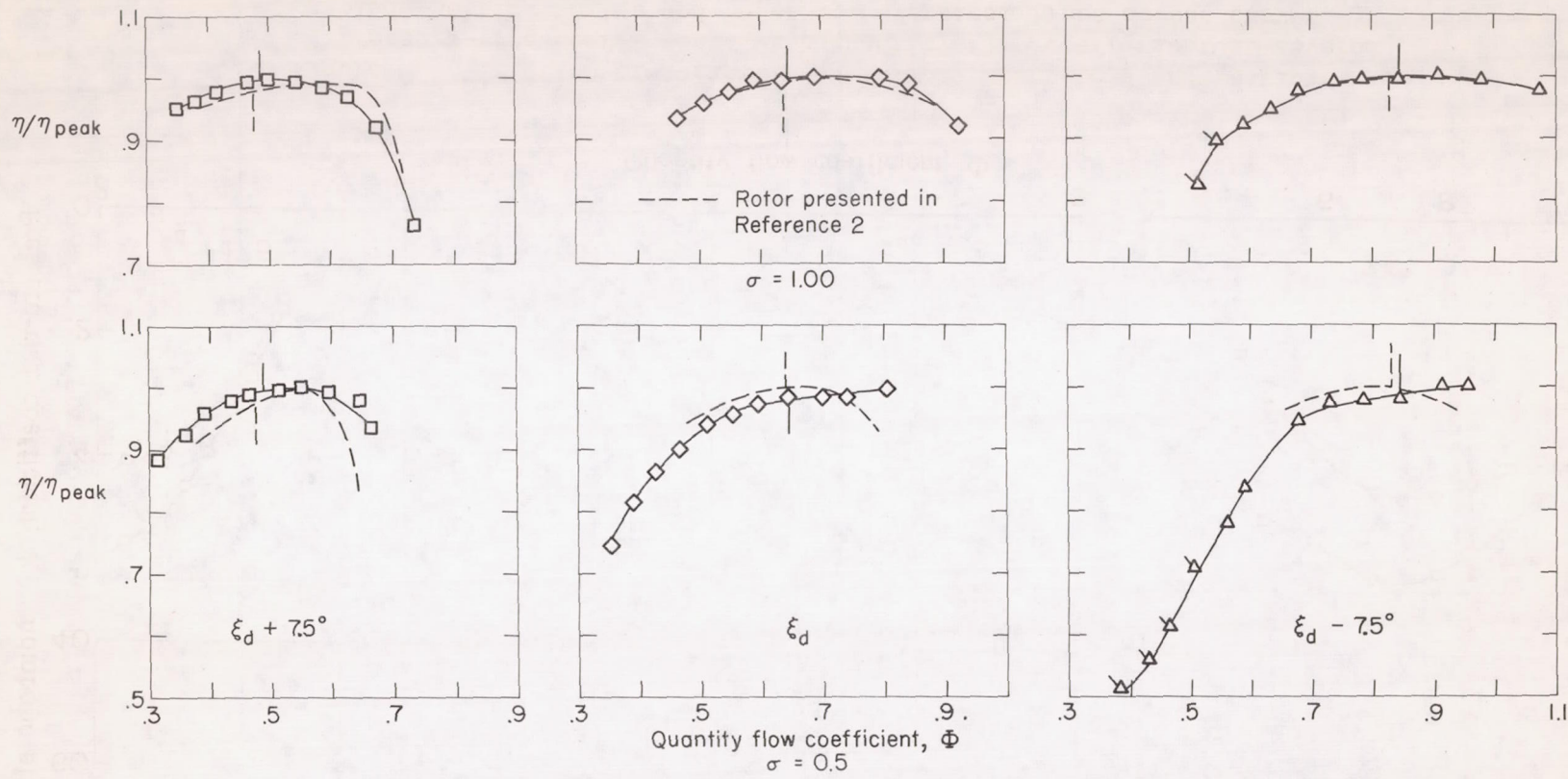
Figure 5.- Comparison of ratio of η/η_{peak} of the rotor of present investigation with that of the rotor reported in reference 2 for three blade-setting angles. Vertical solid and dashed lines indicate design angle of attack. Flagged symbols indicate audible partial-span rotating stall.
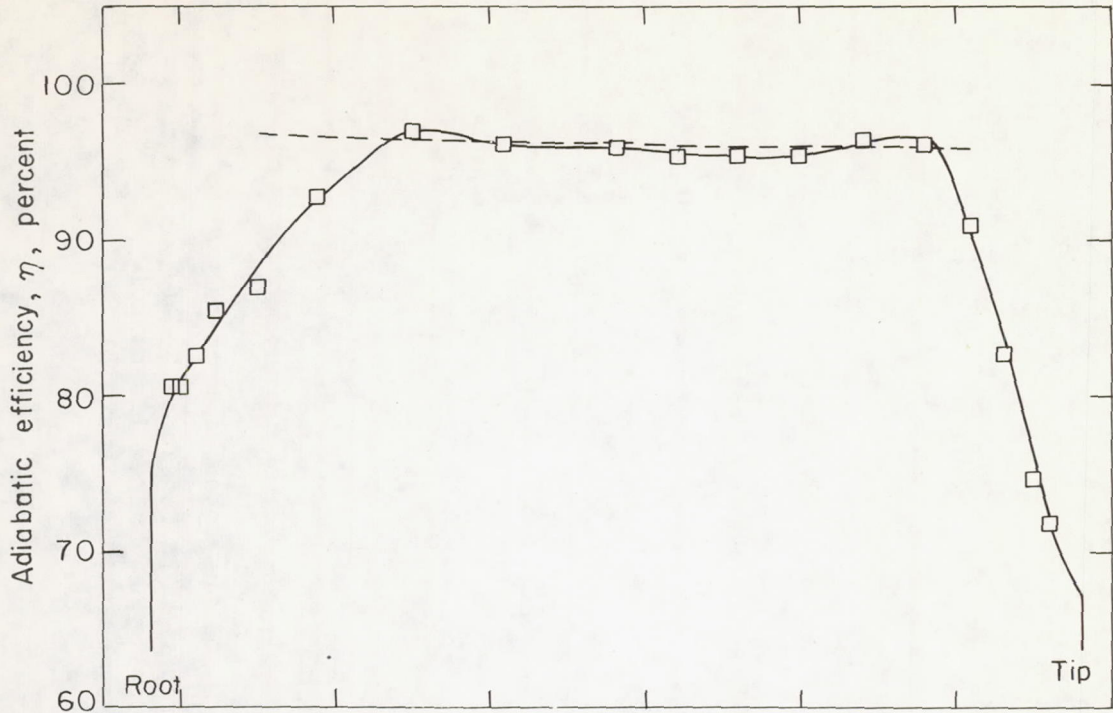
(a) $\xi_d + 7.5°$; $\phi = .502$.
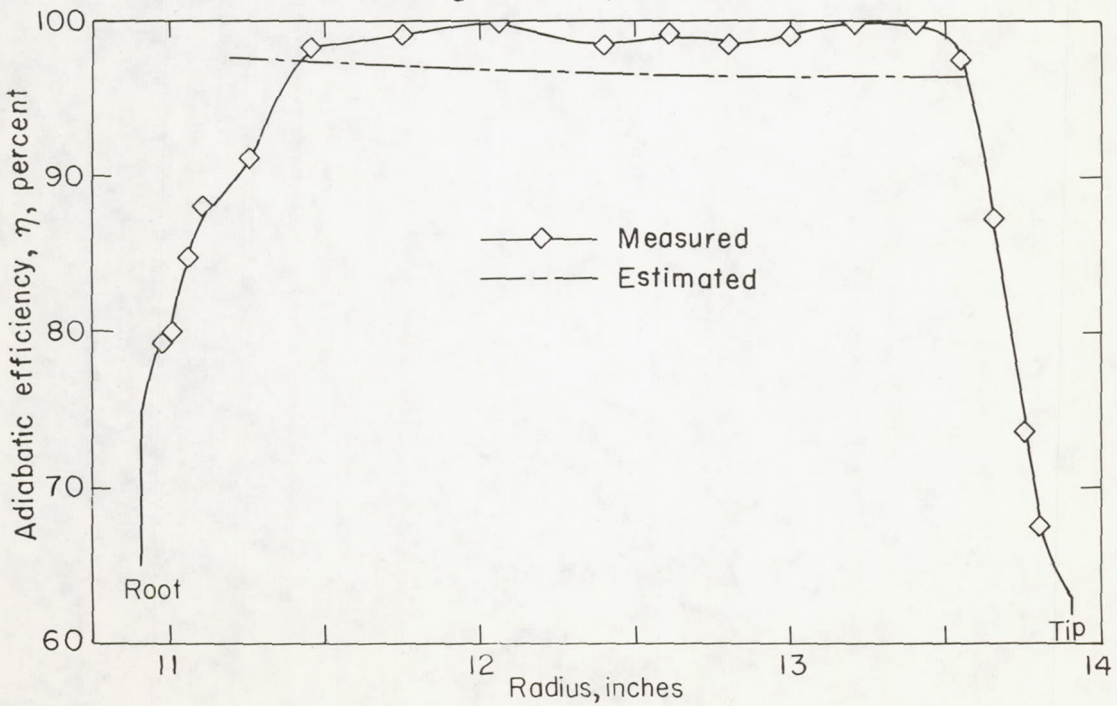
(b) ξ_d ; $\phi = .635$.

Figure 6.- Comparison of measured and estimated blade-element efficiencies across the annulus at $\sigma = 1.0$ and angles of attack close to design.
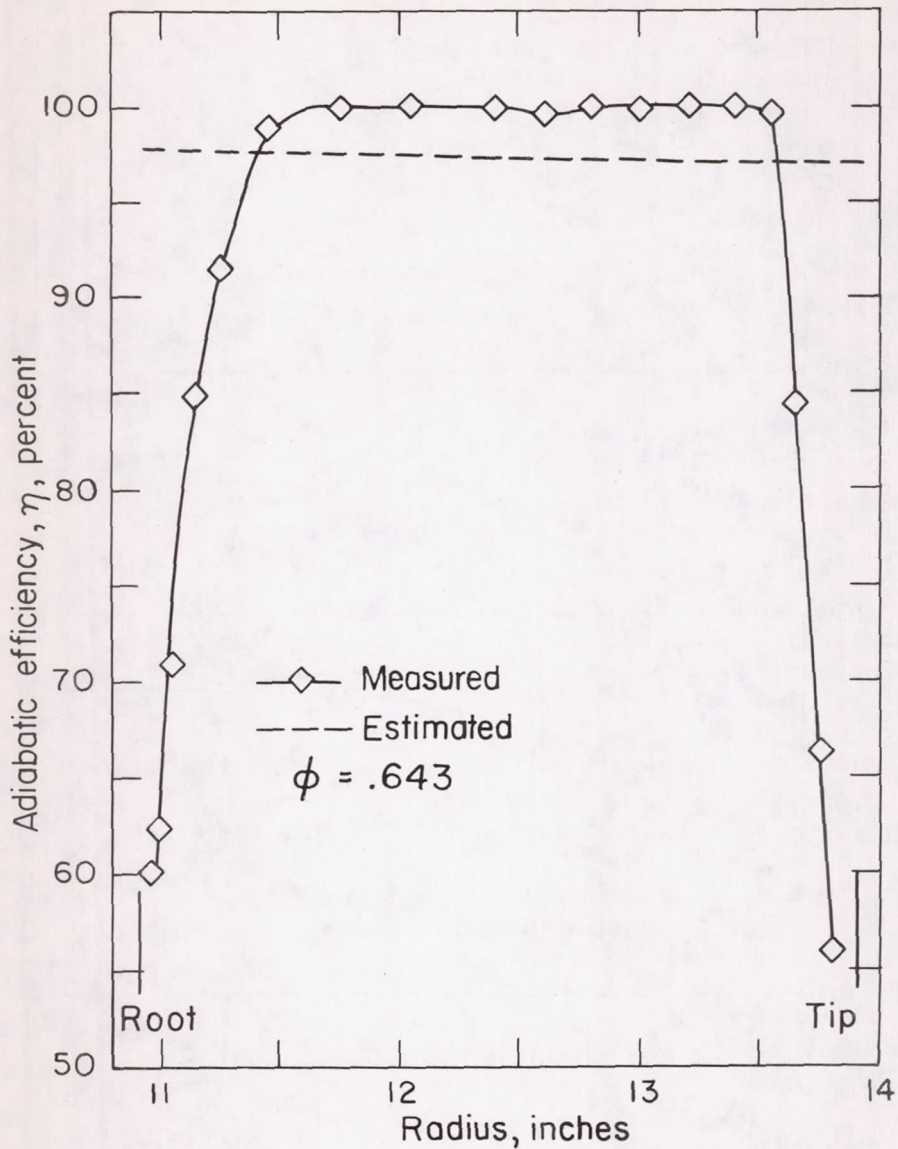
Figure 7.- Comparison of measured and estimated blade-element efficiencies across the annulus at $\sigma = 0.5$ and angle of attack close to design.
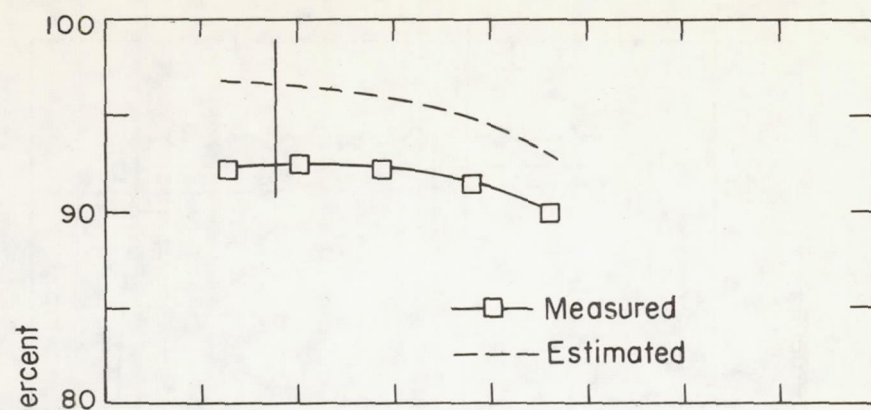
(a) $\xi_d + 7.5°$.
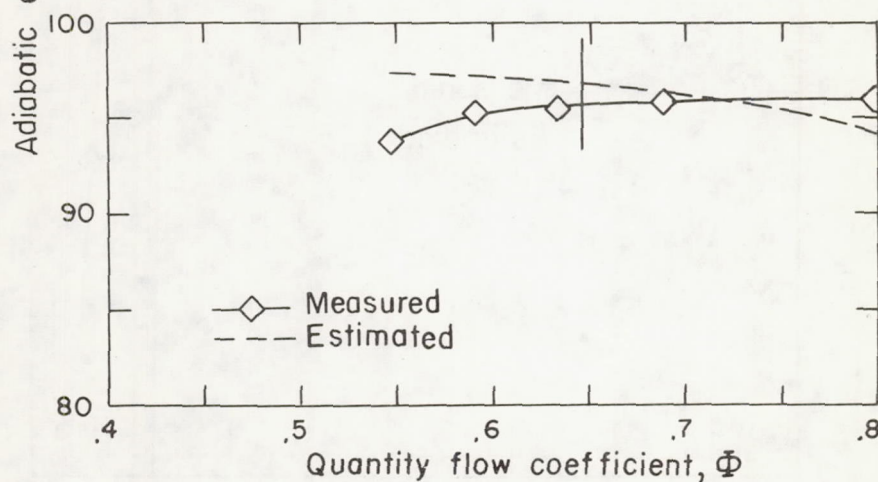
(b) ξ_d.

Figure 8.- Comparison of measured and estimated overall efficiencies for two blade-setting angles at $\sigma = 1.0$. Vertical line across curves indicates design angle of attack.
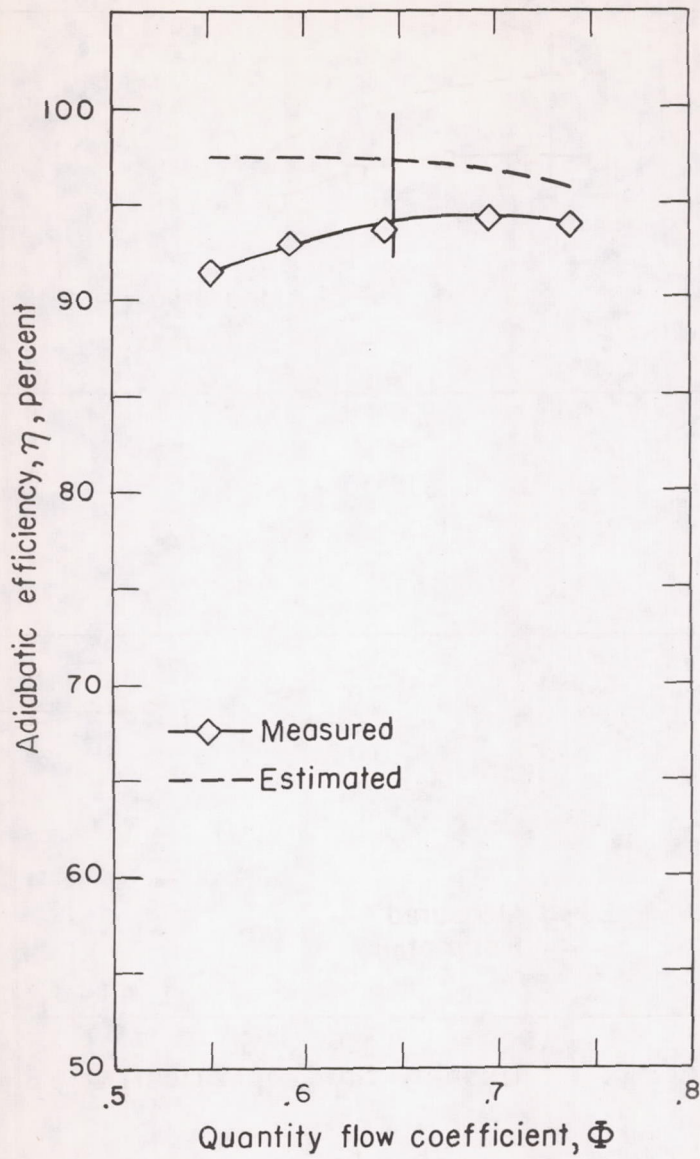
Figure 9.- Comparison of measured and estimated overall efficiencies for ξ_d at $\sigma = 0.5$. Vertical line across curves indicates design angle of attack.
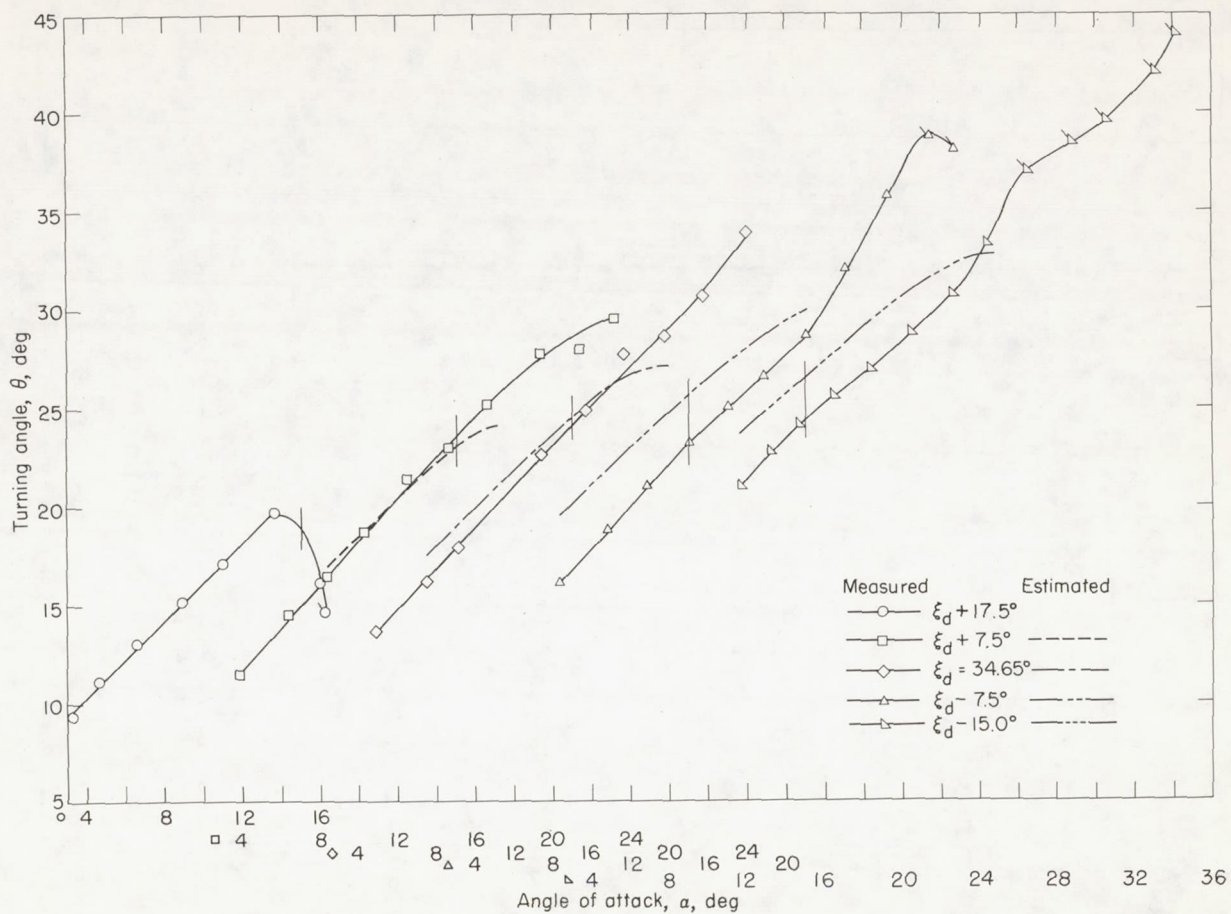
(a) Inboard section; NACA $65(15.8A_{10})10$ section; radius, 11.26 inches.

Figure 10.- Variation of measured and estimated turning angles with angle of attack at three radii for several blade-setting angles and $\sigma = 1.0$. Vertical lines across curves indicate design angle of attack. Flagged symbols indicate audible partial-span rotating stall.
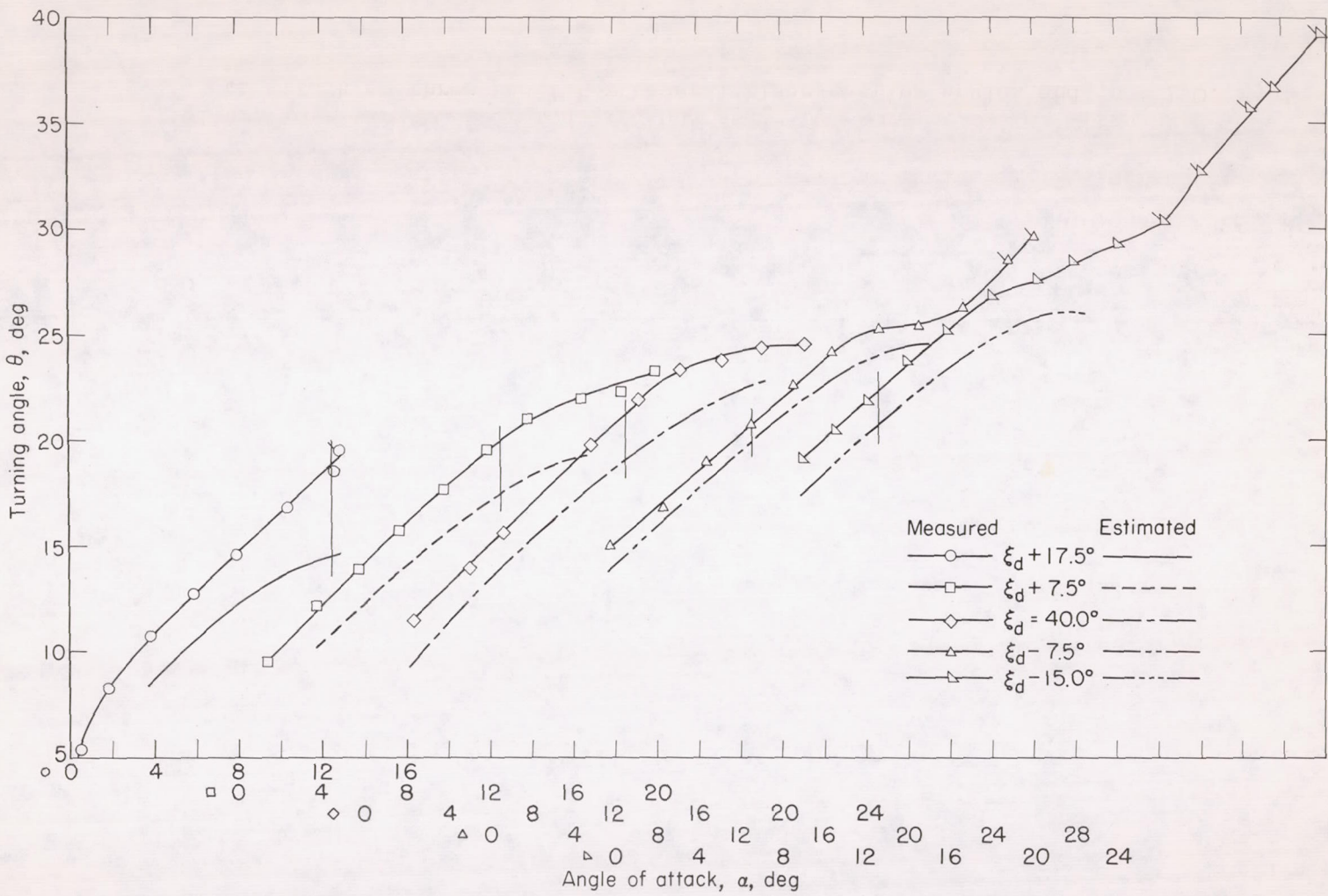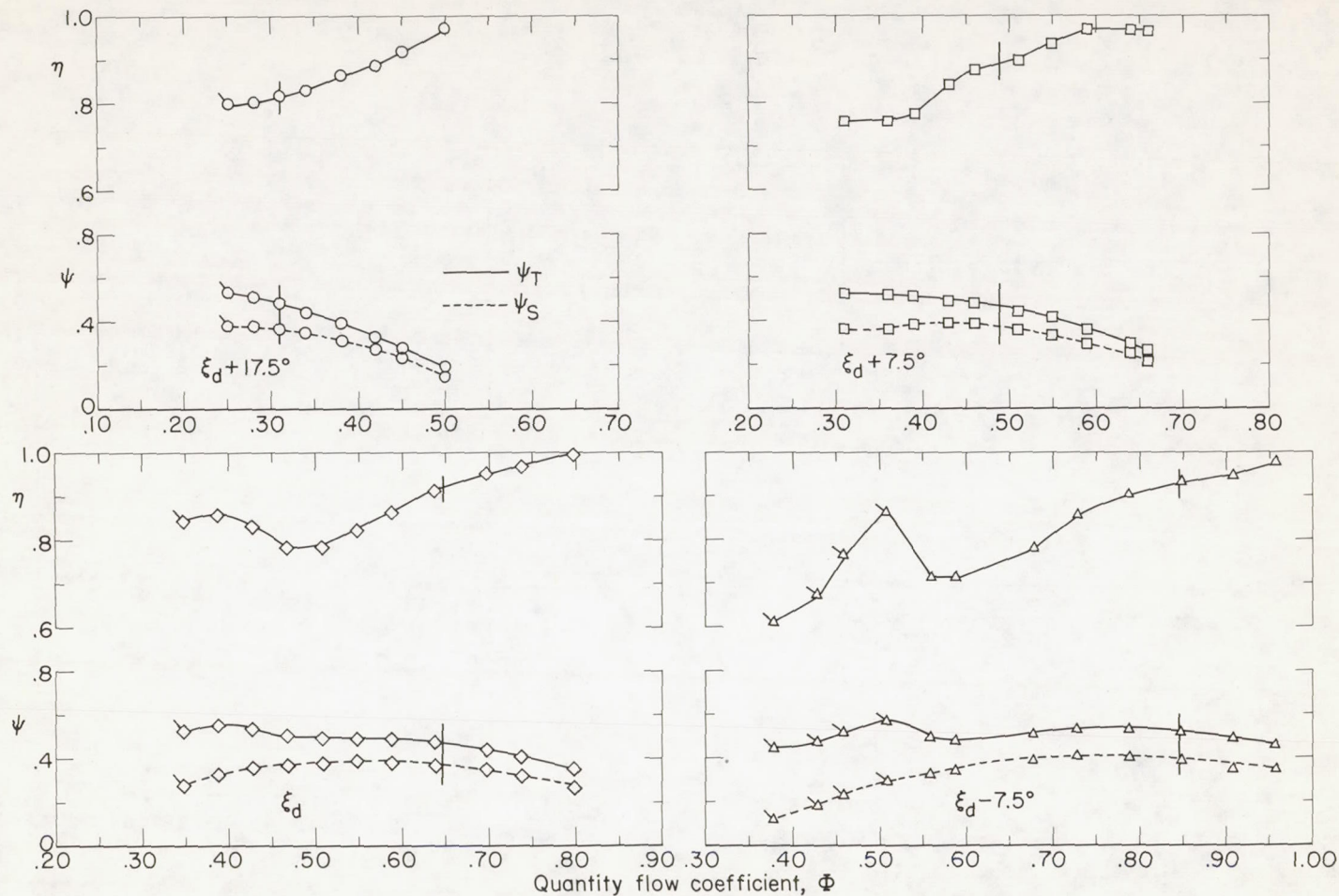
(b) Mean section; NACA $65(12A_{10})10$ section; radius, 12.41 inches.

Figure 10.- Continued.
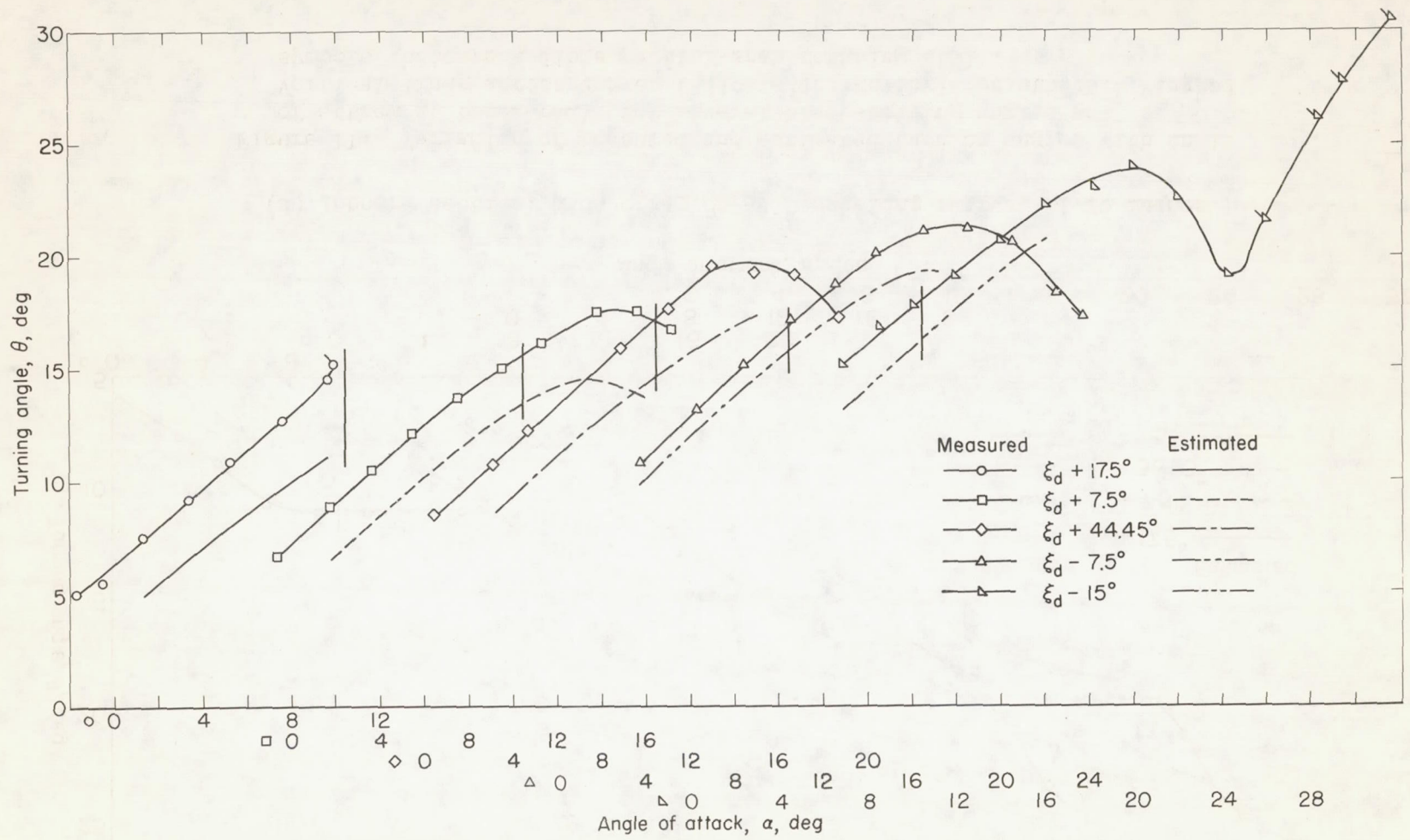
(c) Outboard section; NACA $65(9.3A_{10})10$ section; radius, 13.56 inches.

Figure 10.- Concluded.
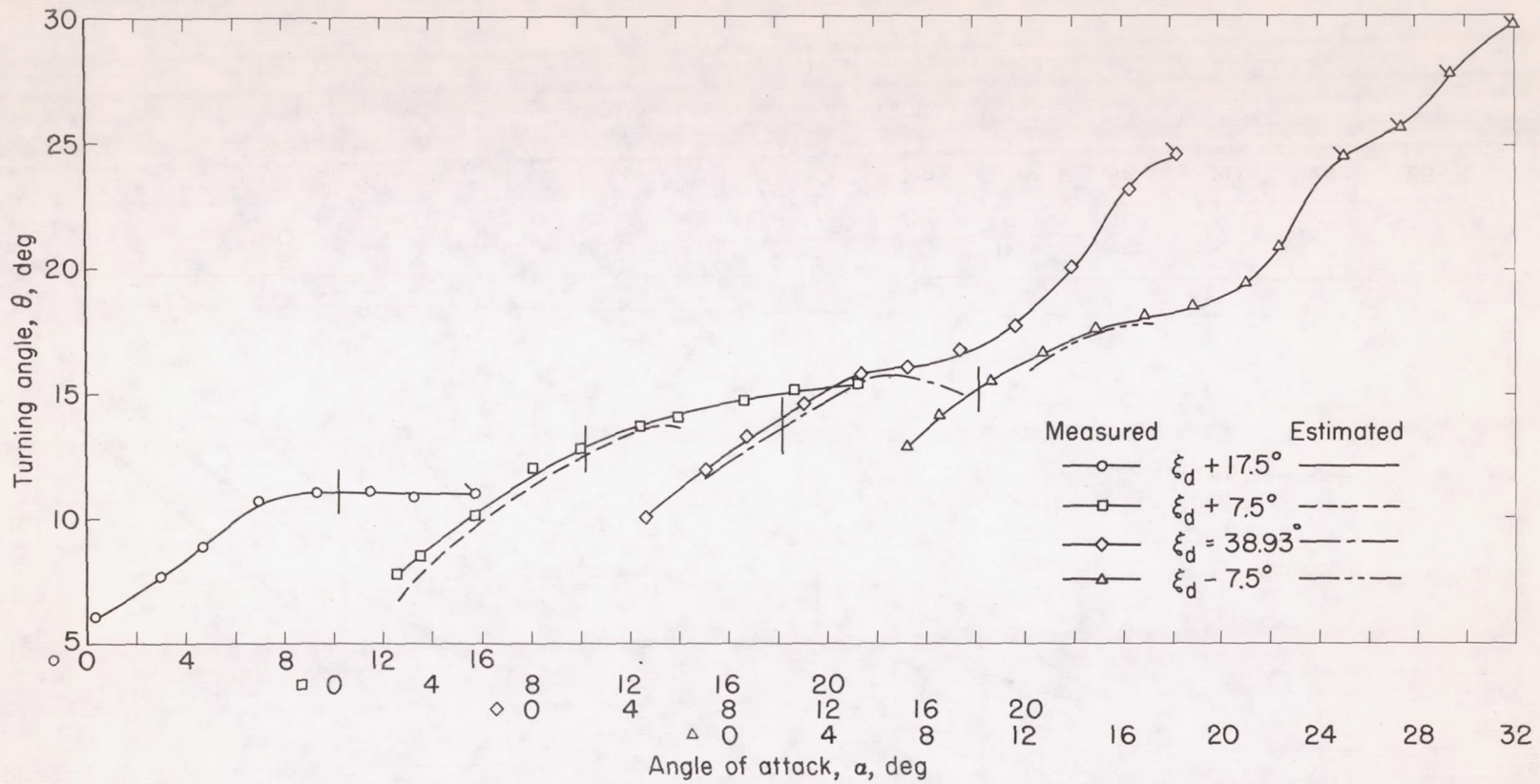
(a) Inboard section; NACA 65(15.8A$_{10}$)10 section; radius, 11.26 inches.

Figure 11.- Variation of measured and estimated turning angles with angle of attack at three radii for several blade-setting angles and $\sigma = 0.5$. Vertical lines across curves indicate design angle of attack. Flagged symbols indicate audible partial-span rotating stall.
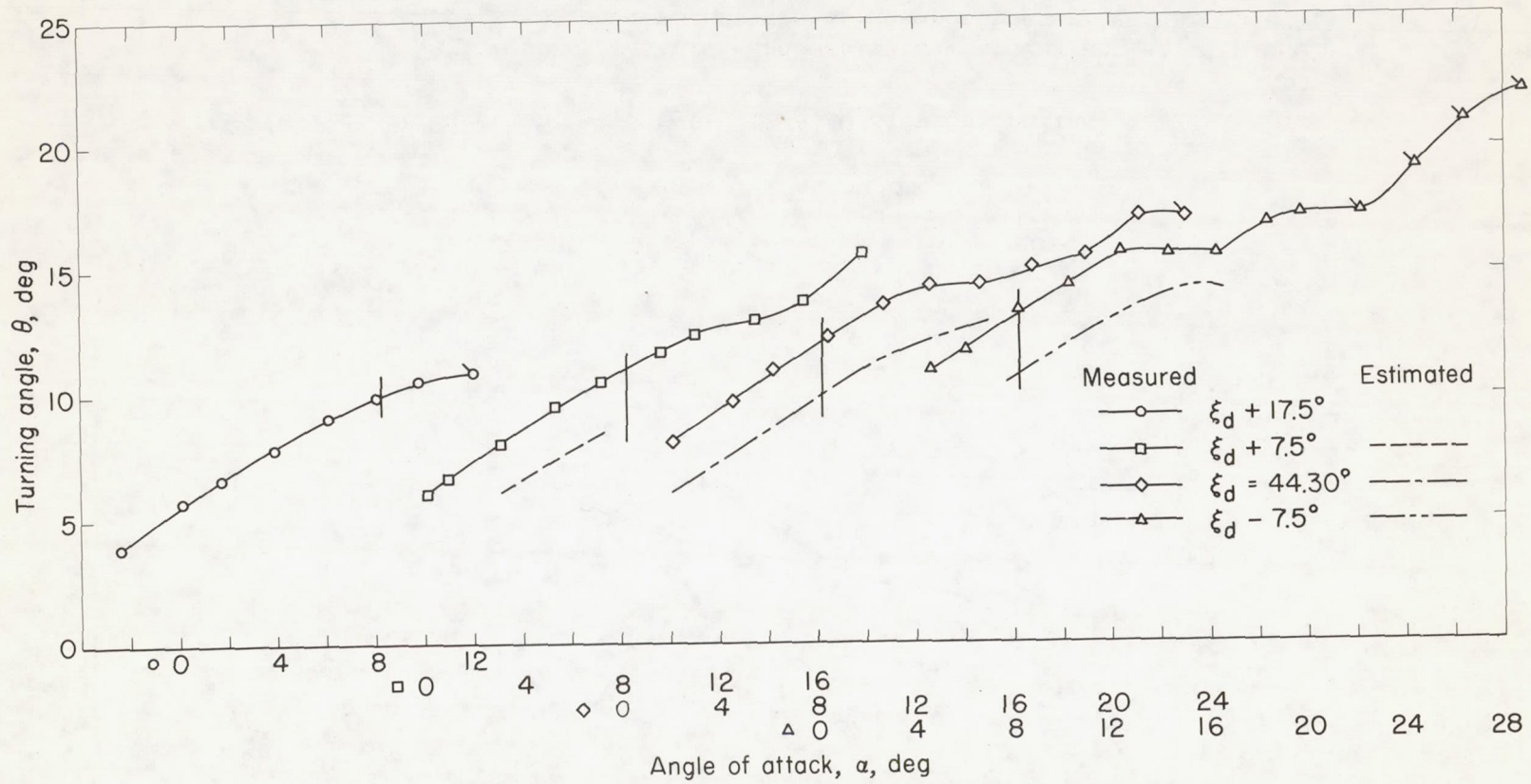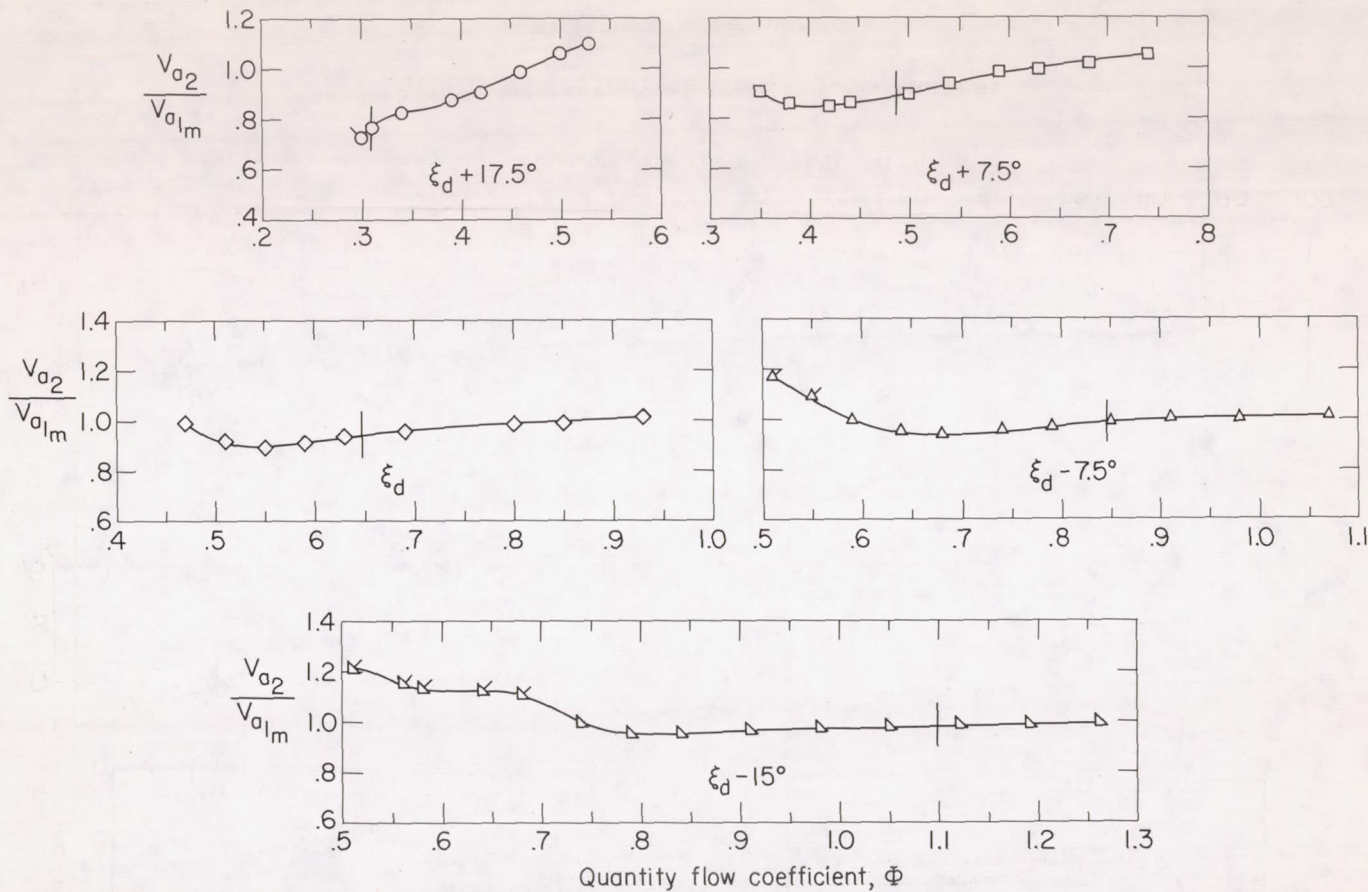
(b) Mean section; NACA 65$\left(12A_{10}\right)$10 section; radius, 12.41 inches.

Figure 11.- Continued.
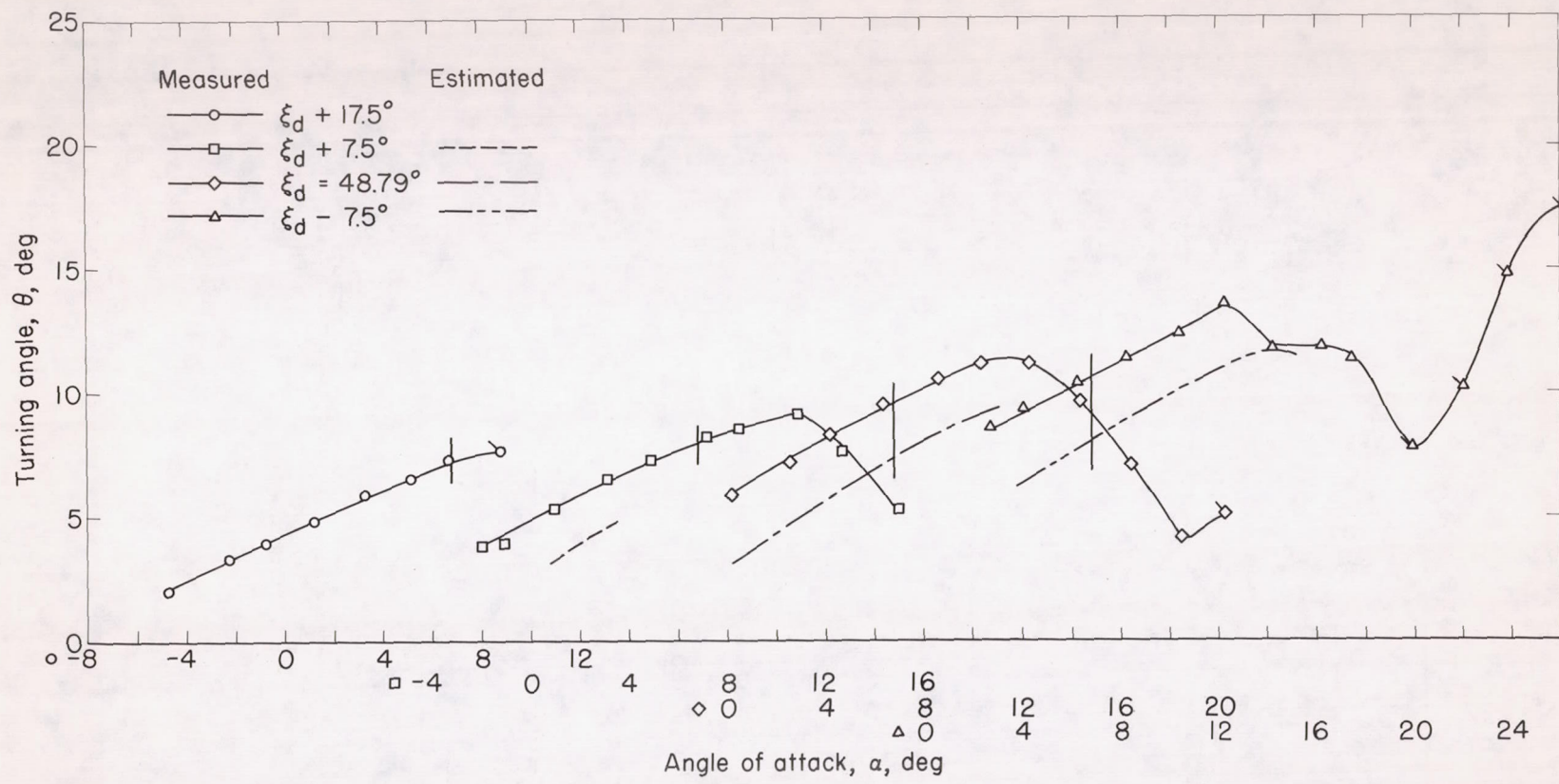
(c) Outboard section; NACA $65\left(9.3A_{10}\right)10$ section; radius, 13.56 inches.

Figure 11.- Concluded.

(a) $\xi_d + 7.5°$.   (b) ξ_d.   (c) $\xi_d - 7.5°$.
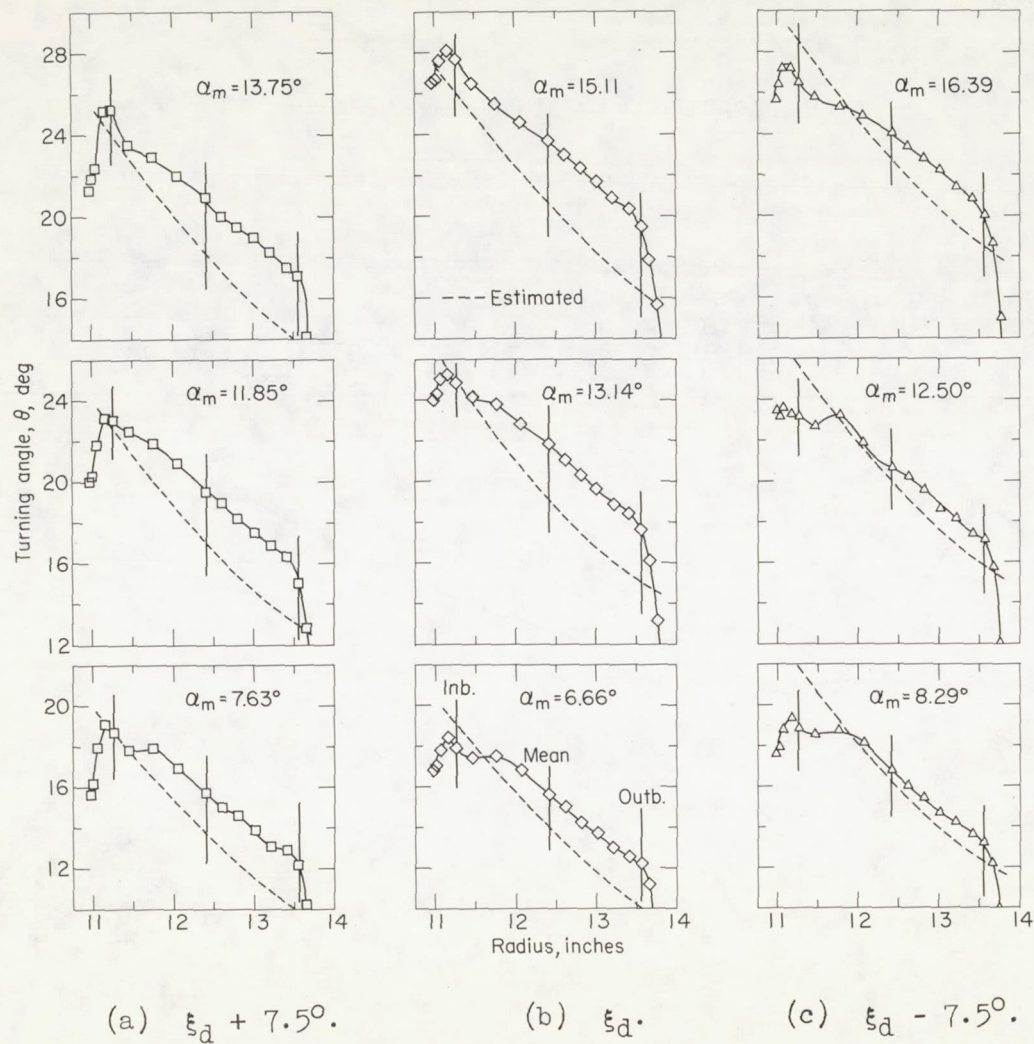
Figure 12.- Radial variation of measured and estimated turning angles at several angles of attack for three blade-setting angles. $\sigma = 1.0$; $\alpha_{d_m} = 12.5°$.
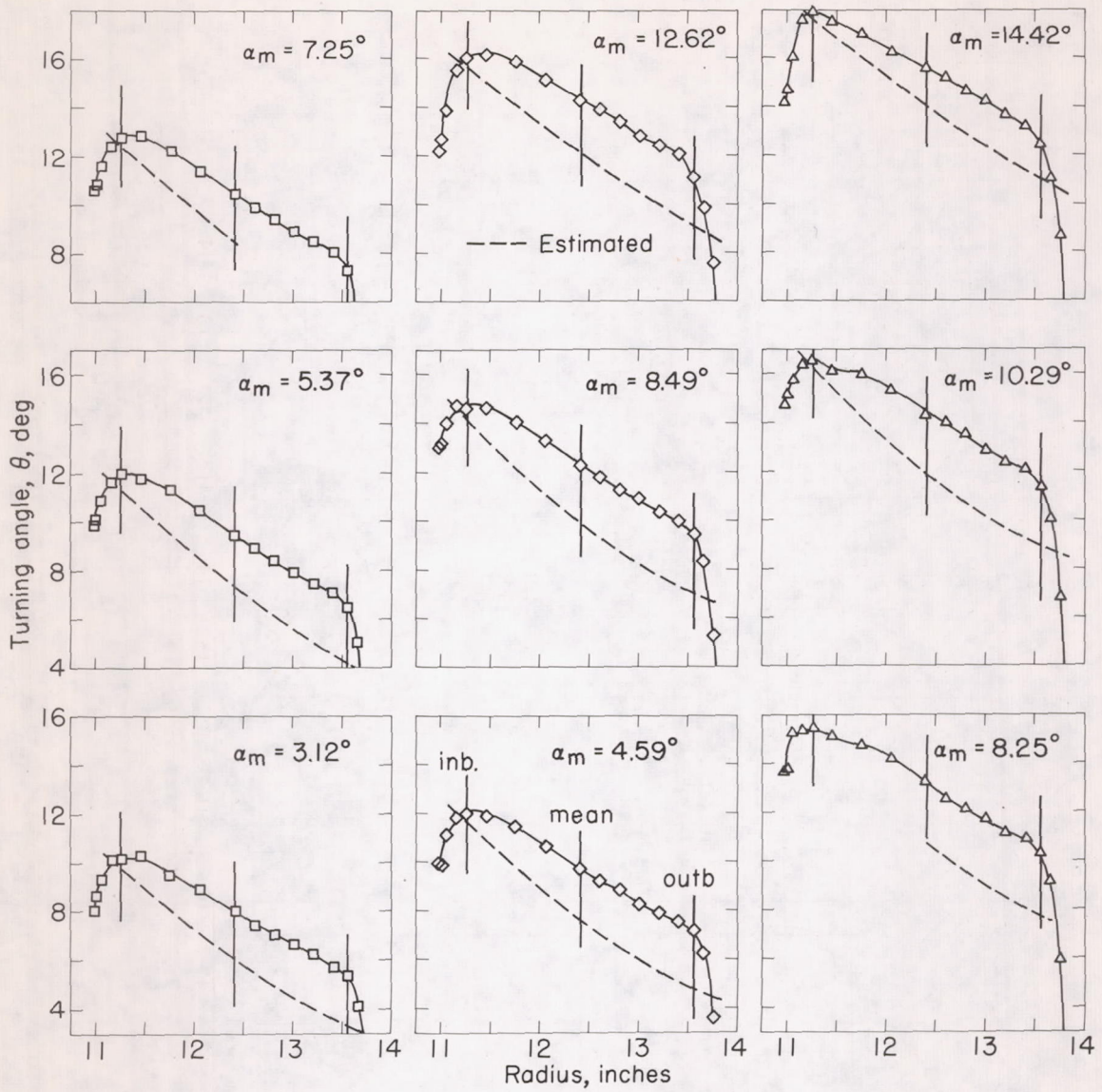
(a) $\xi_d + 7.5°$.   (b) ξ_d.   (c) $\xi_d - 7.5°$.

Figure 13.- Radial variation of measured and estimated turning angles at several angles of attack for three blade-setting angles. $\sigma = 0.5$; $\alpha_{d_m} = 8.3°$.
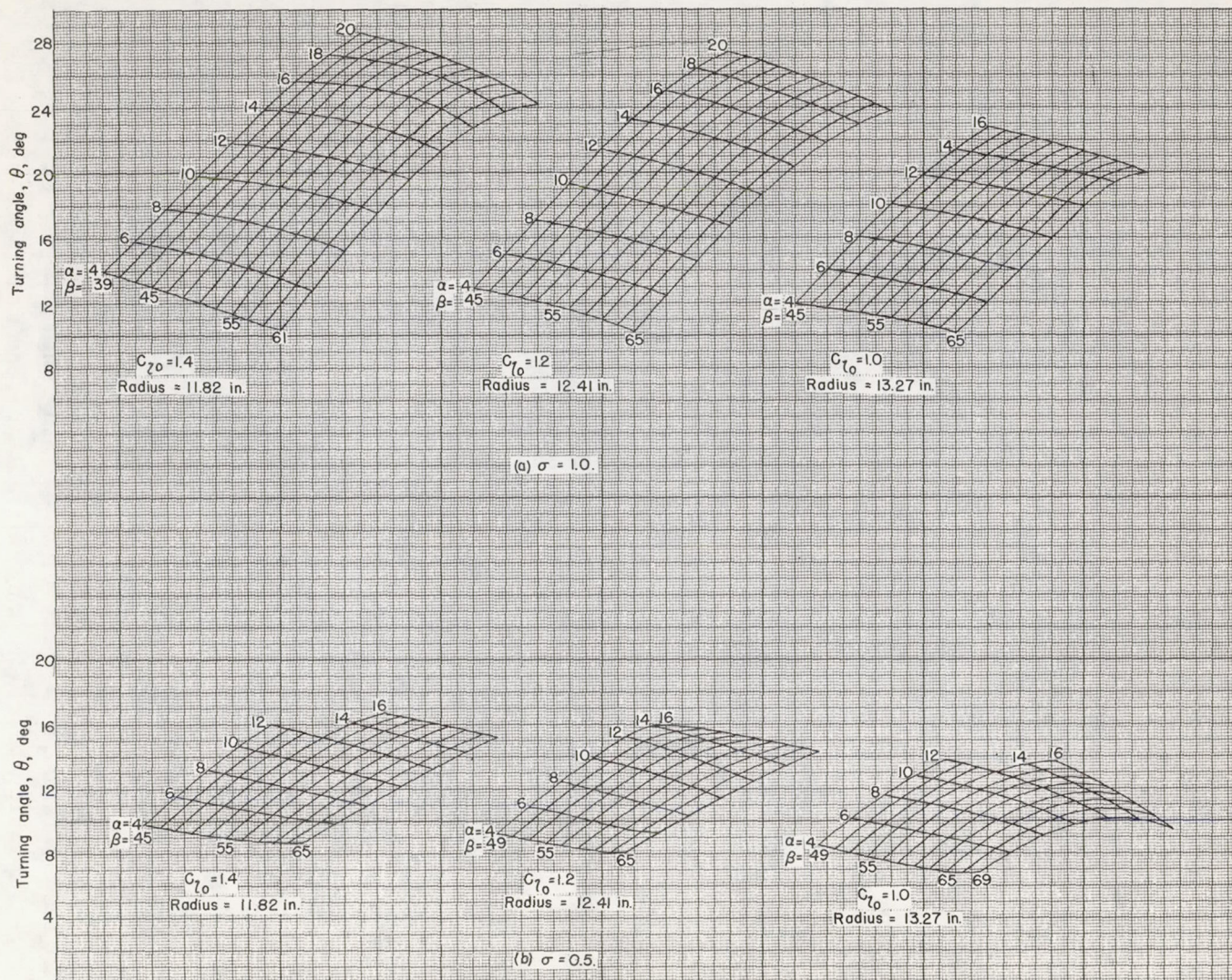
Figure 14.- Variation of turning angle with angle of attack and inlet
angle for three blade sections.
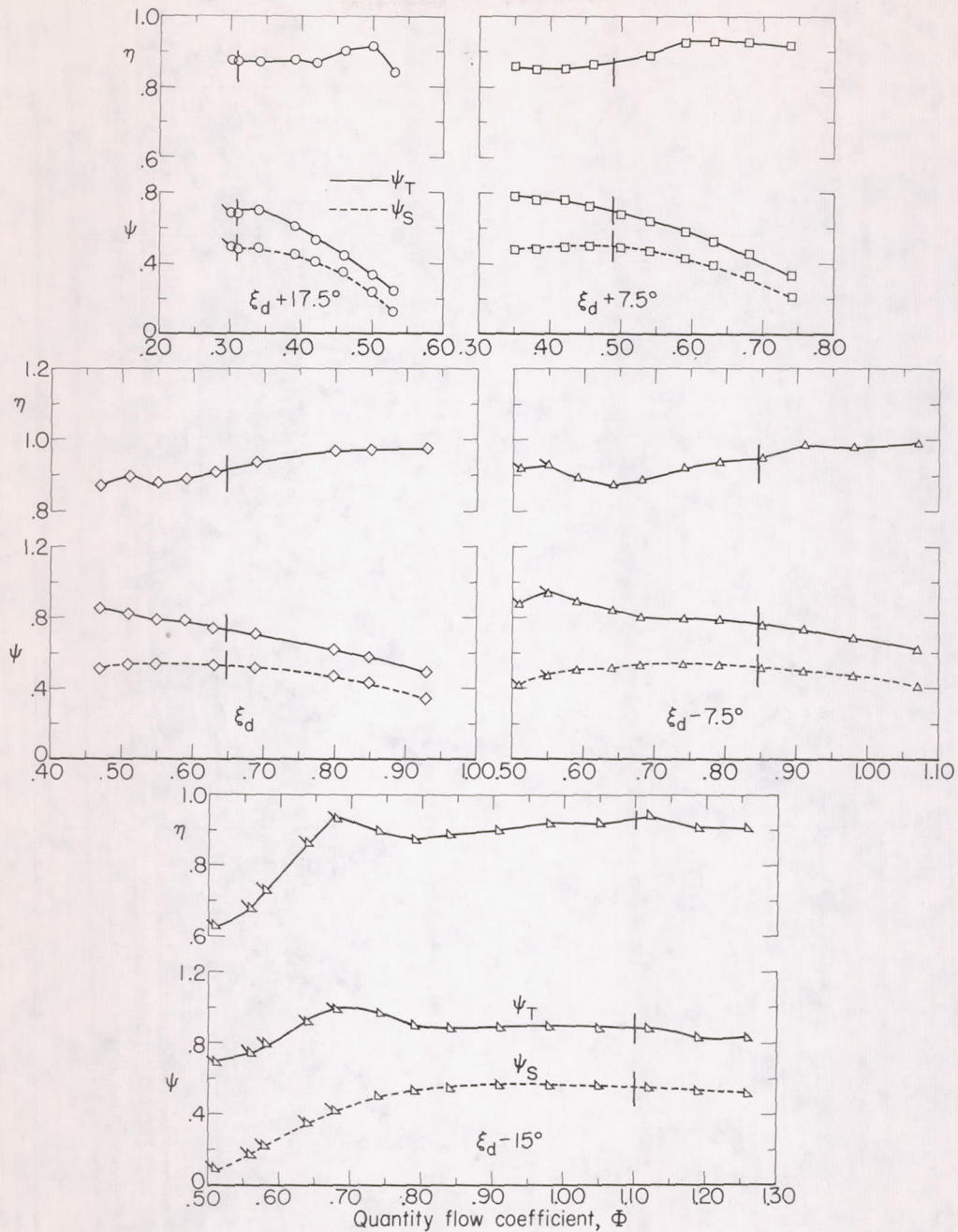
(a) Inboard section; radius, 11.26 inches.

Figure 15.- Variation of efficiency and static- and total-pressure-rise
   coefficients with quantity flow coefficient at three radial stations
   for several blade-setting angles and σ = 1.0. Vertical lines across
   curves indicate design angle of attack. Flagged symbols indicate
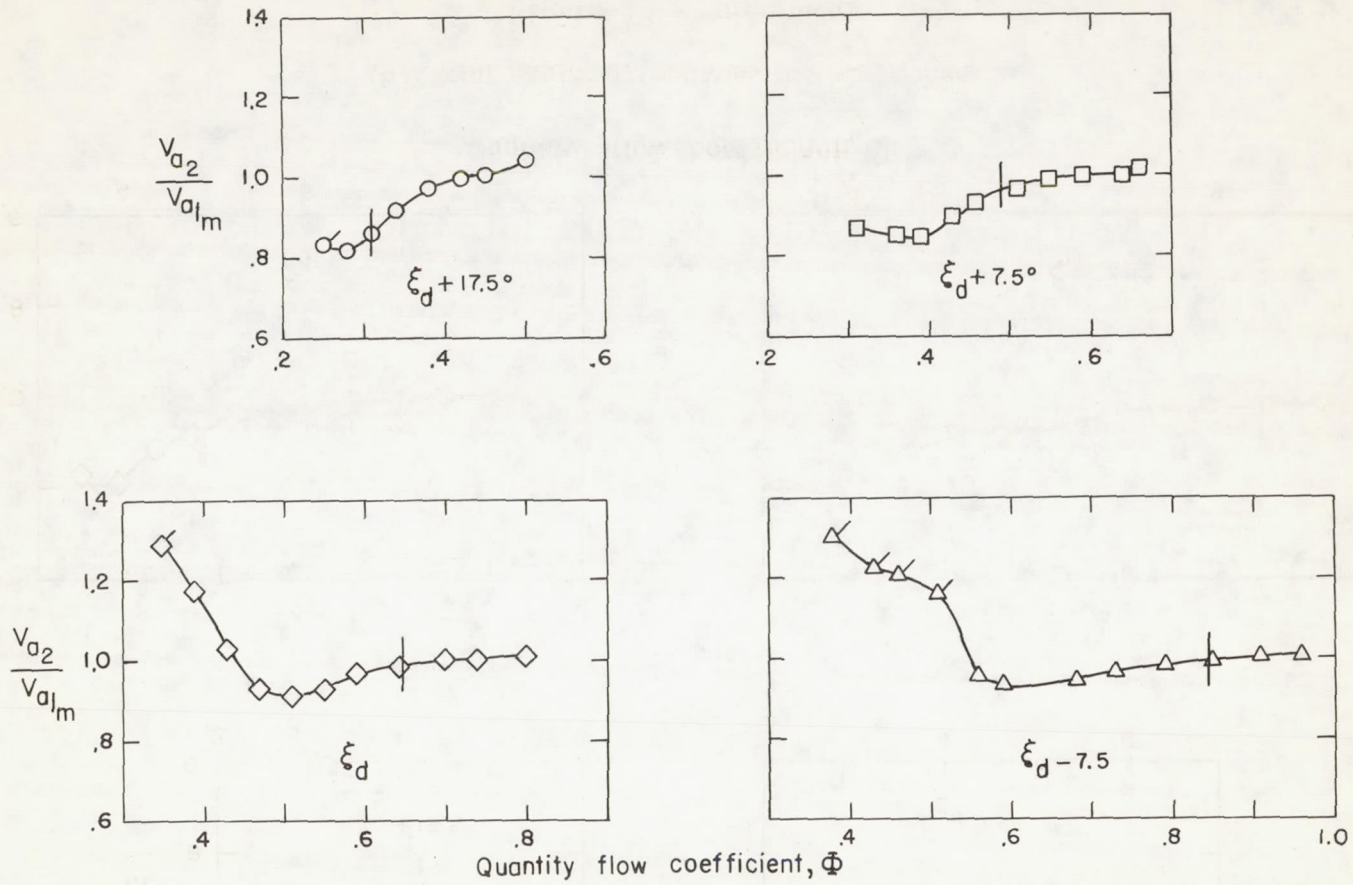   audible partial-span rotating stall.

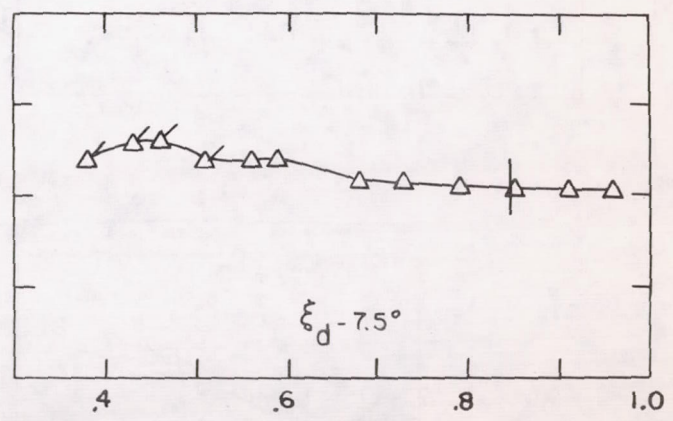(b) Mean section; radius, 12.41 inches.
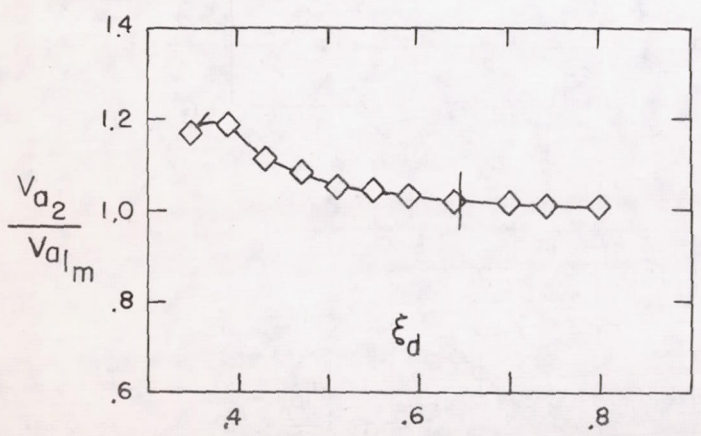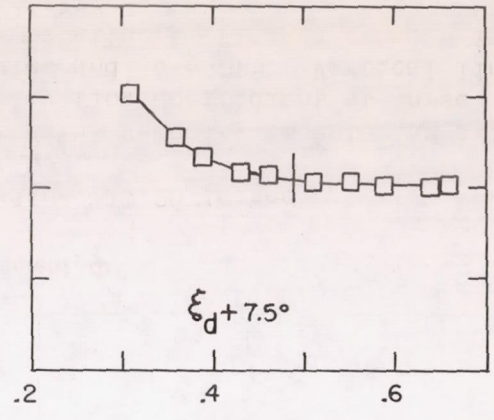
Figure 15.- Continued.
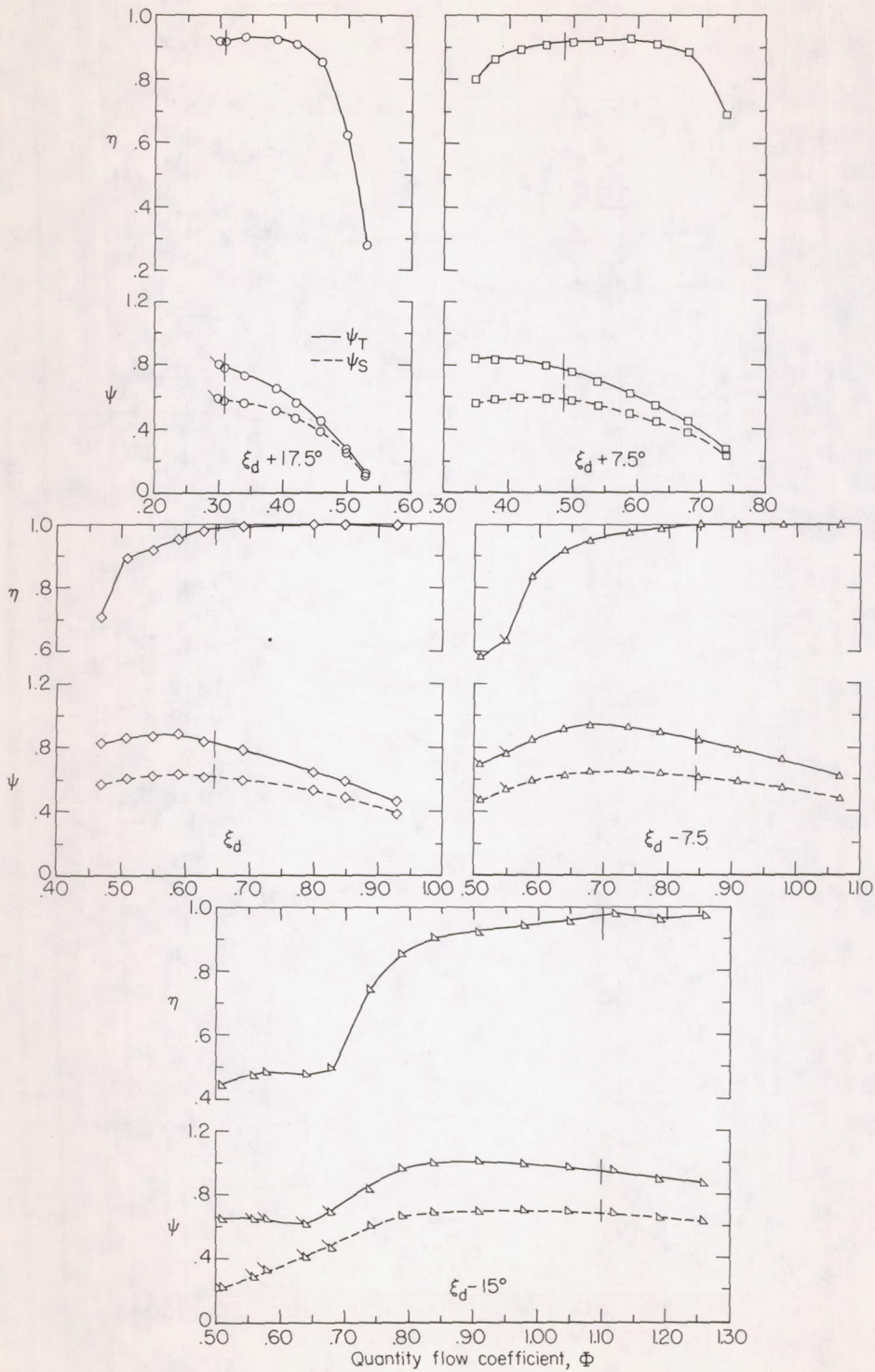
(c) Outboard section; radius, 13.56 inches.

Figure 15.- Concluded.

(a) Inboard section; radius, 11.26 inches.

Figure 16.- Variation of efficiency and static- and total-pressure-rise
coefficients with quantity flow coefficient at three radial stations
for several blade-setting angles and σ = 0.5. Vertical lines across
curves indicate design angle of attack. Flagged symbols indicate
audible partial-span rotating stall.
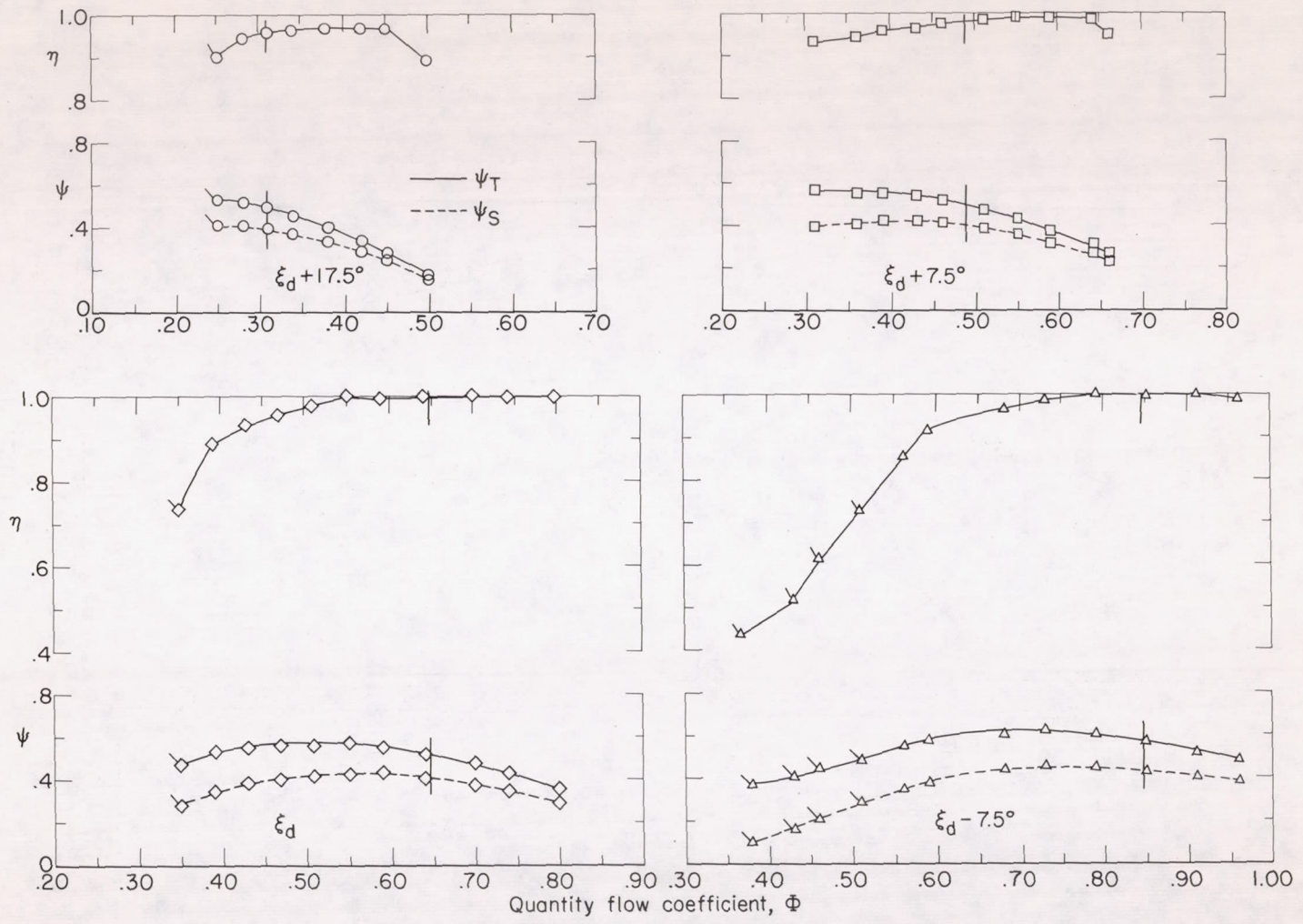
(b) Mean section; radius, 12.41 inches.
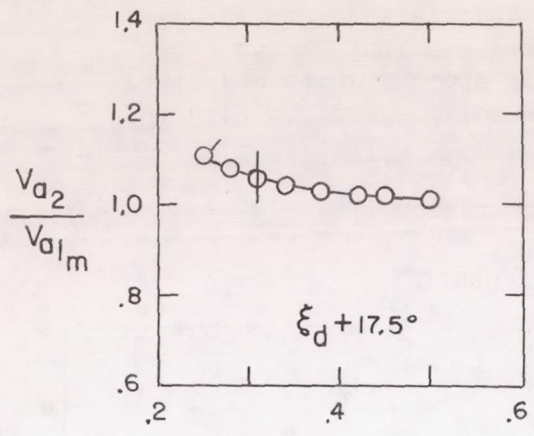
Figure 16.- Continued.
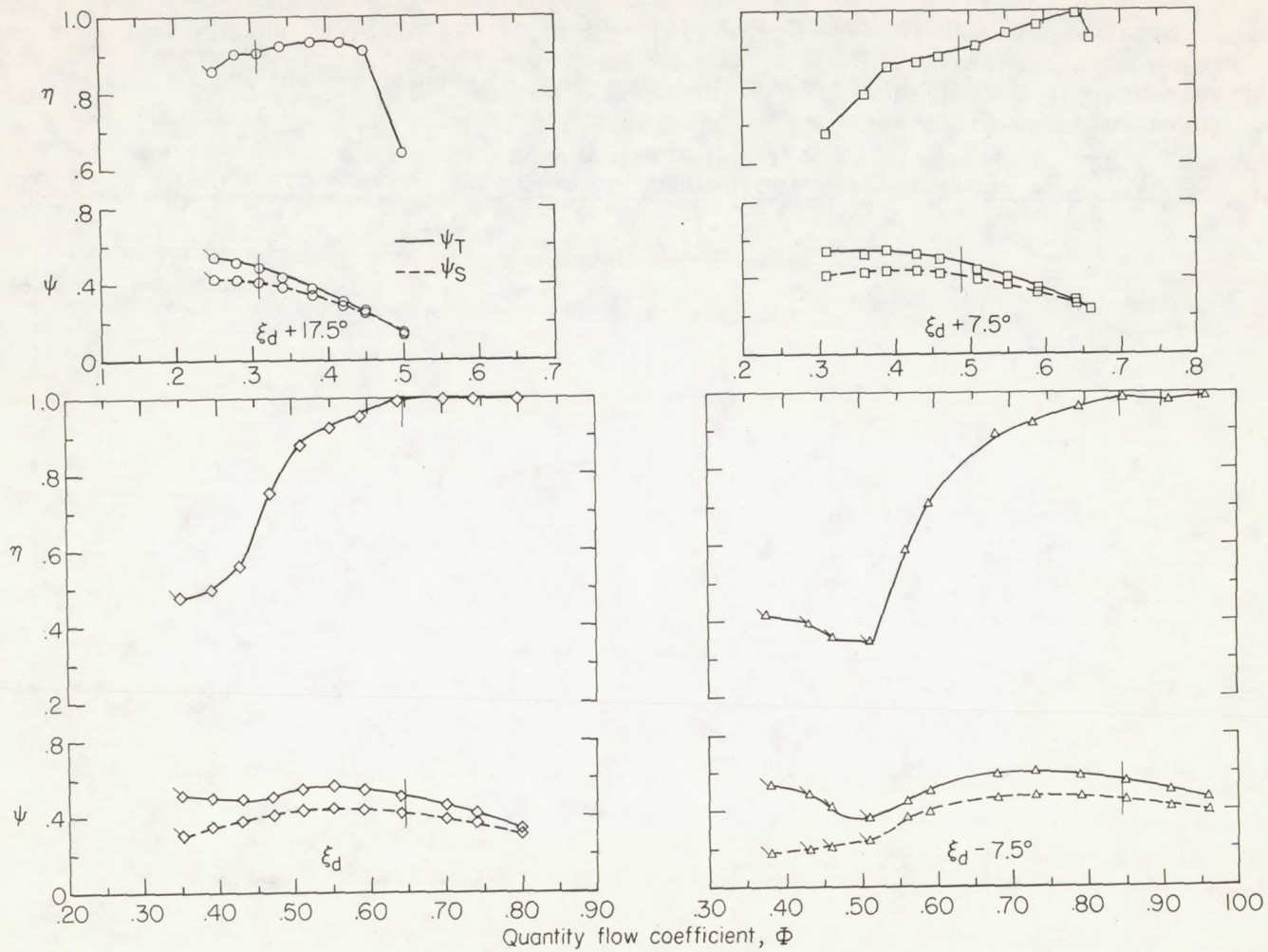
(c) Outboard section; radius, 13.56 inches.

Figure 16.- Concluded.
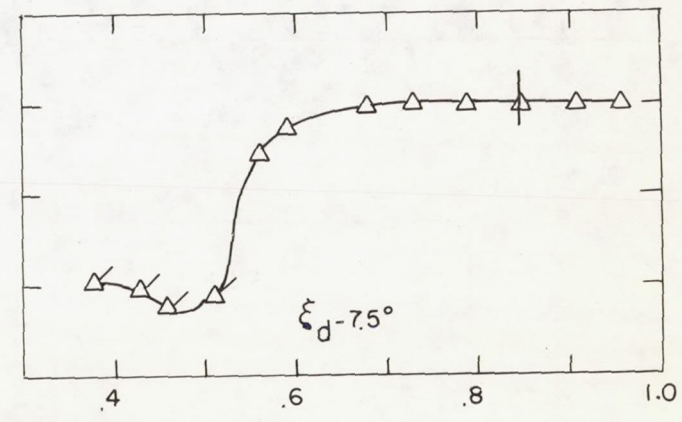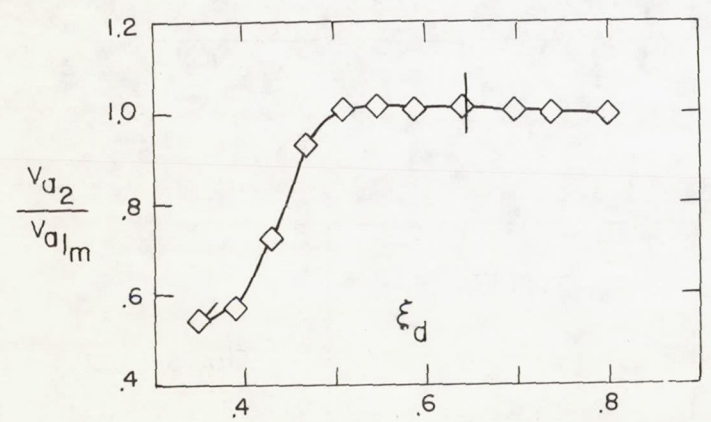
(a) Inboard section; radius, 11.26 inches.

Figure 17.- Variation of ratio of exit axial velocity to entering axial
velocity at mean section with quantity flow coefficient at three radii
for several blade-setting angles and σ = 1.0. Vertical lines across
curves indicate design angle of attack. Flagged symbols indicate
audible partial-span rotating stall.
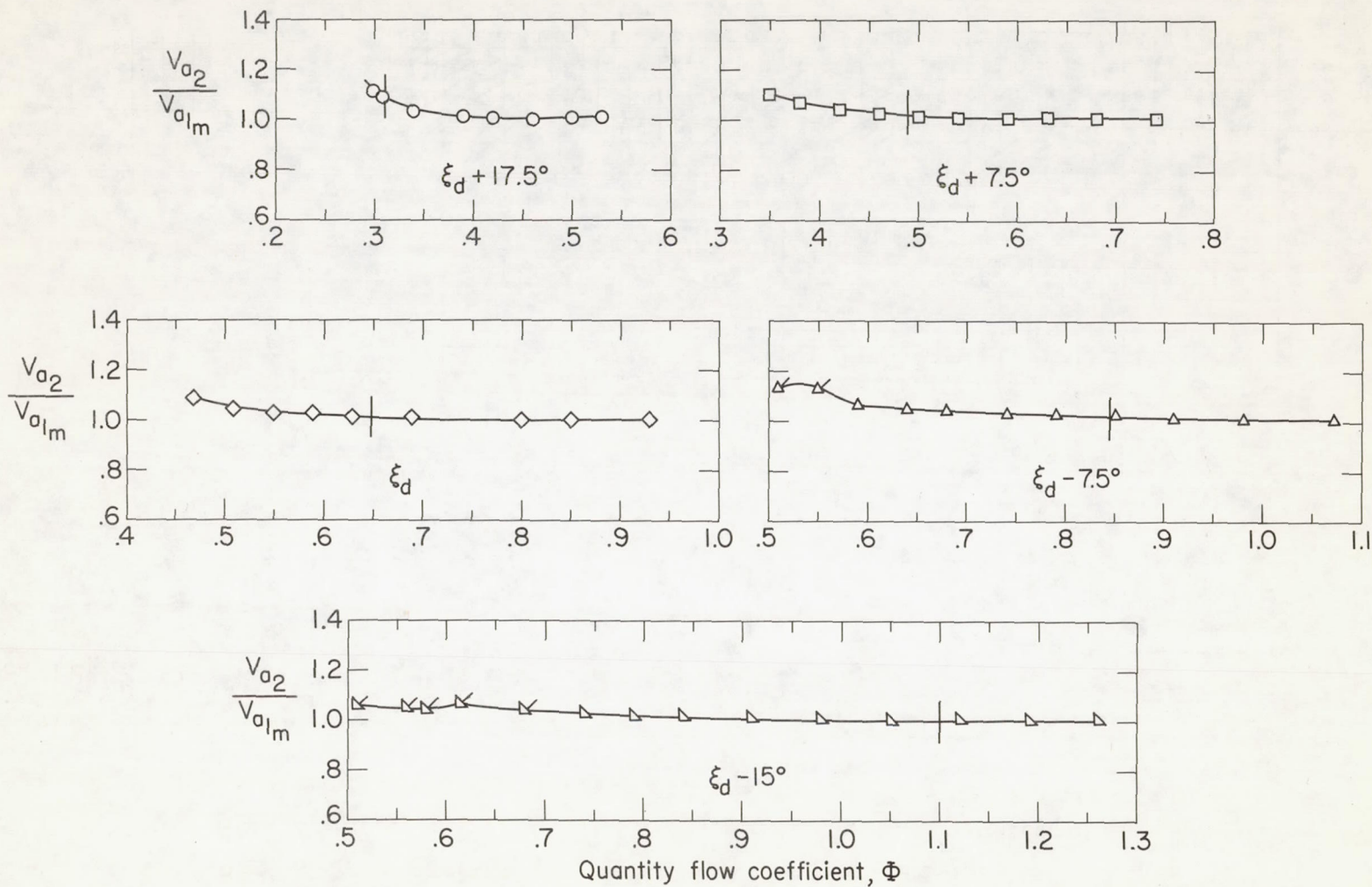
(b) Mean section; radius, 12.41 inches.

Figure 17.- Continued.
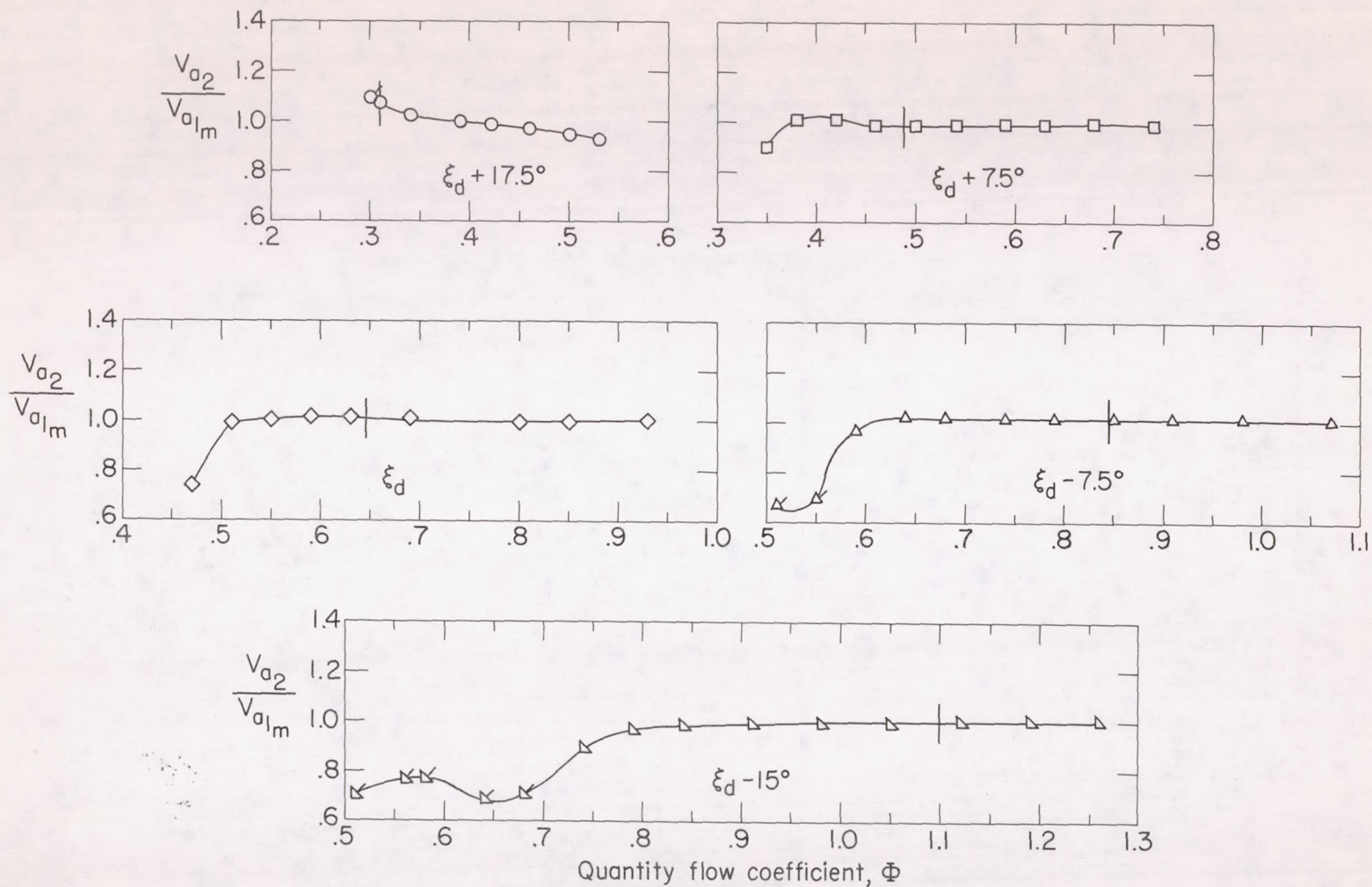
(c) Outboard section; radius, 13.56 inches.

Figure 17.- Concluded.

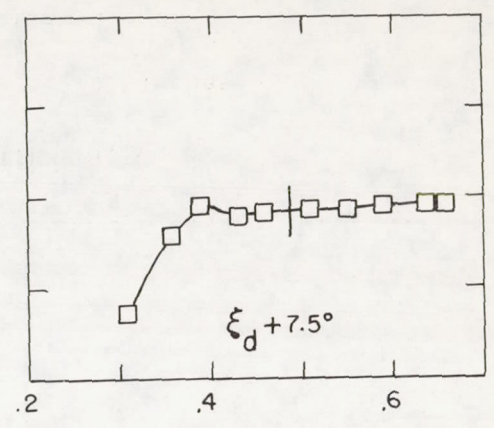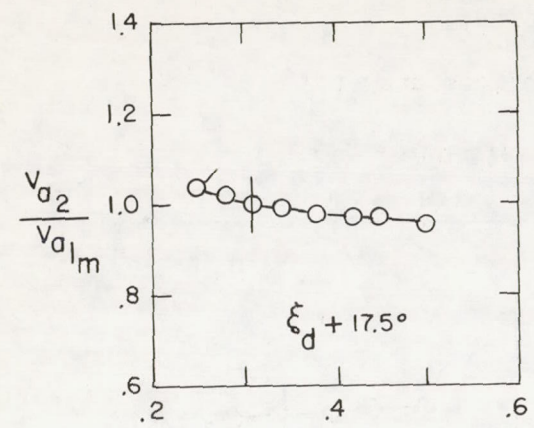(a) Inboard section; radius, 11.26 inches.

Figure 18.- Variation of ratio of exit axial velocity to entering axial velocity at mean section with quantity flow coefficient at three radii for several blade-setting angles and σ = 0.5. Vertical lines across curves indicate design angle of attack. Flagged symbols indicate audible partial-span rotating stall.

(b) Mean section; radius, 12.41 inches.

Figure 18.- Continued.

(c) Outboard section; radius, 13.56 inches.

Figure 18.- Concluded.